Formation and impacts of nitryl chloride in Pearl River Delta

Haichao Wang[1,4], Bin Yuan[2,3,*], E Zheng[2,3], Xiaoxiao Zhang[2,3], Jie Wang[1], Keding Lu[5,6], Chenshuo Ye[2,3], Lei Yang[2,3], Shan Huang[2,3], Weiwei Hu[7], Suxia Yang[2,3], Yuwen Peng[2,3], Jipeng Qi[2,3], Sihang Wang[2,3], Xianjun He[2,3], Yubin Chen[2,3], Tiange Li[2,3], Wenjie Wang[2,8], Yibo Huangfu[2,3], Xiaobing Li[2,3], Mingfu Cai[2,3], Xuemei Wang[2,3], Min Shao[2,3]

[1] School of Atmospheric Sciences, Sun Yat-sen University, Zhuhai, 519082, China

[2] Institute for Environmental and Climate Research, Jinan University, Guangzhou 511443, China

[3] Guangdong–Hong Kong–Macau Joint Laboratory of Collaborative Innovation for Environmental Quality, Guangzhou, 511443, China

[4] Guangdong Provincial Observation and Research Station for Climate Environment and Air Quality Change in the Pearl River Estuary, Key Laboratory of Tropical Atmosphere-Ocean System, Ministry of Education, Southern Marine Science and Engineering Guangdong Laboratory (Zhuhai), Zhuhai, 519082, China

[5] State Key Joint Laboratory of Environmental Simulation and Pollution Control, College of Environmental Sciences and Engineering, Peking University, Beijing, 100871, China.

[6] The State Environmental Protection Key Laboratory of Atmospheric Ozone Pollution Control, College of Environmental Sciences and Engineering, Peking University, Beijing, 100871, China

[7] State Key Laboratory of Organic Geochemistry and Guangdong Key Laboratory of Environmental Protection and Resources Utilization, Guangzhou Institute of Geochemistry, Chinese Academy of Sciences, Guangzhou 510640, China

[8] Multiphase Chemistry Department, Max Planck Institute for Chemistry, Mainz 55128, Germany

Correspondence: Bin Yuan (byuan@jnu.edu.cn)

Abstract. Here we present a field measurement of $ClNO_2$ (nitryl chloride) and N_2O_5 (dinitrogen pentoxide) by a Time-of-Flight Chemical Ionization Mass Spectrometer (ToF-CIMS) with the Filter Inlet for Gas and AEROsols (FIGAERO) at a regional site in Pearl River Delta during a photochemical pollution season from Sept. 26th to Nov. 17th, 2019. Three patterns of air masses are sampled during this campaign, including the dominating air masses from the north and northeast urban regions (Type A), the southeast coast (Type B), and the South China Sea (Type C). The concentration of $ClNO_2$ and N_2O_5 were observed to be much higher in Type A and B than in Type C, indicating that the urban nighttime chemistry is more active than the background marine regions. N_2O_5 uptake coefficient and $ClNO_2$ production yield were estimated based on the field measurement, and the performance of the previously derived parameterizations was assessed. The nighttime $ClNO_2$ correlated with particulate chloride and the mass concentration of fine particles (most likely due to aerosol surface area), suggested that the $ClNO_2$ formation was limited by the N_2O_5 uptake at this site. By examining the relationship between particulate chloride and other species, we implied that anthropogenic emissions (e.g., biomass burning) rather than sea salt particles dominate the origin of particulate chloride, although the site beings only about 100 km away from the ocean. A box model with detailed chlorine chemistry is used to investigate the impacts of $ClNO_2$ chemistry on atmospheric oxidation. Model simulations showed the chlorine radical liberated by $ClNO_2$ photolysis during the next day had a slight increase in concentrations of OH, HO_2 and RO_2 radicals, as well as minor contributions to RO_2 radical and O_3 formation (<5%, on daytime average) in all the three types of air masses. Relative higher contributions were observed in Type A and B. The overall low contributions of $ClNO_2$ to atmospheric oxidation are consistent with those reported recently from wintertime observations in China (including Shanghai, Beijing, Wangdu and Mt. Tai). This may be attributed to: (1) Relative low particle mass concentration limited $ClNO_2$ formation; (2) Other reactions channels, like nitrous acid (HONO), oxygenated volatile organic compounds (OVOCs, including formaldehyde), and ozone photolysis, had more significant radical formation rate during the ozone pollution episodes and weakened the $ClNO_2$ contribution indirectly. The results provided scientific insights into the role of nighttime chemistry in photochemical pollution under various scenarios in coastal areas.

1. Introduction

Chlorine radical is an important oxidant in the tropospheric besides OH radicals, NO_3 radicals and ozone (Saiz-Lopez and von Glasow, 2012; Simpson et al., 2015; Wang et al., 2019b), which alters the fate of many atmospheric compositions, including oxidants, reactive nitrogen compounds, volatile organic compounds (VOCs), and other halogens. Cl radical is much more reactive than OH concerning certain VOCs (e.g., alkanes) by a few orders of magnitude for reaction rate constant (Atkinson and Arey, 2003; Atkinson et al., 2006). therefore, it contributes to atmospheric oxidation capacity considerably in the troposphere despite low concentrations. For example, the global model showed about 20 % of ethane, 14 % of propane oxidation are attributed to chlorine chemistry at the global scale (Wang et al., 2019c). Modeling simulations also demonstrated that chlorine chemistry enhanced oxidative degradation of VOCs by >20% at some locations (Sarwar et al., 2014).

Photolysis of $ClNO_2$ (R1) is a major source of the tropospheric chlorine radical (Thornton et al., 2010b; Simpson et al., 2015), other chlorine radical sources include the reaction of HCl with OH (Riedel et al., 2012; Eger et al., 2019), photolysis of Cl_2 and other halogen compounds like ICl and BrCl (Peng et al., 2021). Tropospheric $ClNO_2$ is not only a critical chlorine activation precursor but also a nocturnal reservoir of reactive nitrogen, which is mainly formed by N_2O_5 heterogeneous reaction on chlorine-containing particles with a branching ratio at nighttime (R2).

$$ClNO_2 + hv \rightarrow Cl + NO_2 \qquad (R1)$$

$$N_2O_5 + H_2O/Cl^- \rightarrow \varphi ClNO_2 + (2-\varphi)NO_3^- \quad (R2)$$
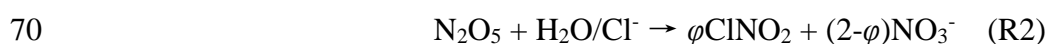
where φ represents the yield of $ClNO_2$. This mechanism was firstly proposed by Finlaysonpitts et al. (1989) through detecting the products of N_2O_5 uptake on NaCl particles. Given this reaction, the formation of $ClNO_2$ can be influenced by the N_2O_5 uptake (such as N_2O_5 uptake probabilities and aerosol surface area) as well as the production yield of $ClNO_2$.

N_2O_5 uptake coefficient, $\gamma(N_2O_5)$, have been reported highly varied under tropospheric conditions (Brown and Stutz, 2012). Both the field and laboratory studies revealed that this process can be affected by ambient temperature, relative humidity (Mozurkewich and Calvert, 1988; Mentel et al., 1999; Hallquist et al., 2003), chemical compositions (such as the content of nitrate, liquid water, chloride, and organics) (Mentel et al., 1999; Brown et al., 2006; Bertram and Thornton, 2009; Gaston et al., 2014; McDuffie et al., 2018b; Tang et al., 2014; Anttila et al., 2006), as well as particle morphology (Mielke et al., 2013; Zong et al., 2021). Until now, the key factors that controlling N_2O_5

uptake coefficient in the different environments are still not well understood. $ClNO_2$ yield is also highly varied subject to the liquid water and chloride content in the aerosol (Behnke et al., 1997; Roberts et al., 2009; Bertram and Thornton, 2009). Several studies demonstrated that the $ClNO_2$ yield is also affected by other factors like aerosol sulfate (Staudt et al., 2019) and organics (Ryder et al., 2015; Tham et al., 2018; McDuffie et al., 2018a). However, the comprehensive quantitative relationship of these factors in controlling the yield still has large uncertainties. These gaps in parameterization of N_2O_5 uptake coefficients and $ClNO_2$ yield result in challenging to accurately predict $ClNO_2$ and particulate nitrate production.

Osthoff et al. (2008) and Thornton et al. (2010a) directly observed elevated $ClNO_2$ in coastal and inland U.S. by chemical ionization mass spectrometer (CIMS), respecitively. They shed light on the significance of $ClNO_2$ photolysis in launching the radical chemistry during the morning time, and also affecting halogen chemistry and reactive nitrogen cycling. Large amounts of chlorine radicals are liberated through the photolysis of noctural accumulated $ClNO_2$ (R1), which oxidizes VOCs and produces peroxy radicals (RO_2) to initiate the daytime raidcal cycling in the morning, when other radical source, like ozonolysis and photolysis of O_3, HONO and HCHO, are still weak (Osthoff et al., 2008). The impacts of $ClNO_2$ chemistry on primany source of radicals and ozone formation is a critical topic, the answer of which is very helpful to narrow the gap of the missing priamry source of ROx and improve our knowledge of the currect ozone pollution mechanism (Tan et al., 2017; Tham et al., 2016). Model simulation highlighted $ClNO_2$ chemistry could increase mean daily maximum 8 h ozone by up to 7.0 ppbv in some areas in the Northern Hemisphere (Sarwar et al., 2014). The large contribution was also confirmed in the southern California region by a box model study (Riedel et al., 2014). In addition, global model simualtion showed $ClNO_2$ chemistry increases wintertime ozone by up to 8 ppb over polluted continents (Wang et al., 2019c). Particularly, previously modelling results also highlight the importance of $ClNO_2$ chemistry in enhancing O_3 production in China (Li et al., 2016; Yang et al., 2022b).

Several field studies reported the measurement of $ClNO_2$ in varied environments in the past decade (Riedel et al., 2012; Young et al., 2012; Mielke et al., 2013; Riedel et al., 2013; Bannan et al., 2015; Faxon et al., 2015; Mielke et al., 2015; Phillips et al., 2016; Bannan et al., 2017; Wang et al., 2017c; Wang et al., 2017d; Le Breton et al., 2018; McDuffie et al., 2018a; Yun et al., 2018a; Zhou et al., 2018; Bannan et al., 2019; Eger et al., 2019; Haskins et al., 2019; Jeong et al., 2019; Xia et al., 2020; Xia et al., 2021; Tham et al., 2016; Tham et al., 2014; Wang et al., 2016; Phillips et al., 2012; Lou et al., 2022; Sommariva et al., 2018), in which the maximum $ClNO_2$ up to sub-ppbv to several ppbv were reported, indicating its ubiquitous presence worldwide and a broad atmospheric impacts over various regions. During the CalNex-LA campaign 2010, $ClNO_2$ was measurred at ground site,

116   the Research Vessel and aircraft platform, which depicted a full picture of the abundance of $ClNO_2$

117   and confirmed its large impacts on atmospheric chemsitry in both urban and coastal regions in

118   California (Riedel et al., 2012; Young et al., 2012; Mielke et al., 2013). Recently, Wang et al. (2016)

119   used a box model simulated the chemical evolution of the plume after leaving the observation site in

120   Hongkong and showed $ClNO_2$ chemistry had a following-day enhancement of ozone peak and

121   daytime ozone production rate by 5–16% and 11–41%, along with a large increasing of OH, HO_2 and

122   RO_2 concentration especially in the morning. While Xia et al. (2021) and Lou et al. (2022) reported

123   winter measurments of $ClNO_2$ in north and east China, respectively, they both showed moderate

124    $ClNO_2$ level and a relative small contributions of $ClNO_2$ chemistry to radical source and ozone

125   enhancement on campaign average. These results is quite different with that happened during the

126   summertime in China (Tham et al., 2016; Wang et al., 2016; Tan et al., 2017), and highlight the large

127   variation of $ClNO_2$ chemistry influenced by temporal spatial distribution.

128   Despite its likely importance to the regional atmospheric oxidation and air quality, investigations

129   of $ClNO_2$ chemistry in China remain relatively sparse. There are several field measurements of

130    $ClNO_2$ conducted in the China in recent years, while considering the large diversities of air mass in

131   inland and coastal regions in China, more field and model works are need to gain more insights to

132   the $ClNO_2$ chemistry in various atmospheric environments and assess its atmospheric impacts. Until

133   now, only several field measurement of $ClNO_2$ were reported in Pearl River Delta (PRD) region

134   (Tham et al., 2014; Wang et al., 2016; Yun et al., 2018a), and only Wang et al. (2016) reported a

135   comprehensive analysis of the impact of $ClNO_2$ chemistry on radical and ozone formation in 2013 as

136   mentioned before. To understanding the increasing O_3 problem in recent years (Wang et al., 2019a)

137   and examining the role of $ClNO_2$ chemistry in O_3 formation in PRD, we measured $ClNO_2$, N_2O_5, and

138   other related parameters at a regional site in PRD during a severe photochemical pollution season in

139   2019. The abundance, formation, and variation during different air masses patterns are well

140   characterized. The factors impact its formation are diagnosed. Finally, the contribution of chlorine

141   radicals liberated by $ClNO_2$ photolysis on the daytime radical chemistry, as well as ozone formation

142   are comprehensively assessed by a box model coupled with detailed chlorine chemistry.

143   **2. Method**

144   **2.1 Measurement site**

145   This campaign was conducted at the Guangdong Atmospheric Supersite of China, which is located

146   on the top of a mountain (~ 60 m high, a.s.l.) in Heshan (22.728°N, 112.929°E), Jiangmen city,

147   Guangdong Province (Yang et al., 2022a) . This site was in the western Peral River Delta where no

148   major industry in the surroundings, but with some farmland and a few residents live at the hill foot.

149   The traffic is far away from this site and believed to have little influence on the sampling. The

150   anthropogenic activity is much lower than the urban regions like Guangzhou City, but the air quality

151   is often influenced by neighbor cities, especially the outflow of air masses from the regions on the

152   north and northeast. Therefore, the air masses sampled at this site are sometimes representative of the

153   urban pollution from the center PRD. There were many atmospheric intensive studies once

154   conducted in the site to study the air pollutions in PRD (Tan et al., 2019; Yun et al., 2018b). In this

155   study, the instruments were located on the top floor of the measurement building with inlets

156   approximately 15 m above the ground. The data presented in the study were collected from 27th

157   September to 17th November 2019, during which photochemical pollution occurred frequently (Yang

158   et al., 2022a). Time is given as CNST (Chinese National Standard Time = UTC+8 h). During the

159   campaign, sunrise was approximately at 06:00 and sunset was approximately at 18:00 CNST.

160   **2.2 Instrument setup**

161   A comprehensive suite of instrumentation was overviewed and listed in Table 1. An iodide-adduct

162   Time-of-Flight Chemical Ionization Mass Spectrometer (ToF-CIMS) with the Filter Inlet for Gas and

163   AEROsols (FIGAERO) was applied to measure $ClNO_2$ and N_2O_5 along with other oxygenated

164   organic species (Ye et al., 2021; Wang et al., 2020b) . In brief, the gas phase species were measured

165   via a 2-m-long, 6-mm-outer-diameter PFA inlet while the particles were simultaneously collected on

166   a Teflon filter via a separate 2-m-long, 10-mm-outer-diameter copper tubing inlet; both had flow

167   rates of 2 L min^{-1} with a drainage flow of 20 L min^{-1}. The gas phase was measured for 25 minutes at

168   1 Hz, and the FIGAERO instrument was then switched to place the filter in front of the ion molecule

169   region; it was then heated incrementally to 200 °C to desorb all the mass from the filter to be

170   measured in the gas phase, which resulted in high-resolution thermograms. $ClNO_2$ and N_2O_5 are

171   measured as the iodide adduct ions at m/z 207.867 ($IClNO_2^-$) and m/z 234.886 ($IN_2O_5^-$) in the ToF-

172   CIMS, respectively. The measurement background and sensitivities for detecting $ClNO_2$ and N_2O_5

173   with the dependence of water content were quantified (see Appendix). The limit of detection (LOD)

174   for $ClNO_2$ and N_2O_5 were 4.3 and 6.0 pptv in 1-minute time-resolution, respectively, with an

175   uncertainty of ~30%.

176   Sub-micron aerosol composition (PM_1) were measured by a High-Resolution Time of Flight

177   Aerosol Mass Spectrometer (HR-ToF-AMS) (DeCarlo et al., 2006). The soluble ions of sodium and

178   potassium was measured by a commercial instrument (GAC-IC) equipped with an aerosol collector

179   and detected by ion chromatography (Dong et al., 2012). The particle number size distribution

180   (PNSD) was measured by a scanning mobility particle sizer (SMPS, TSI 3938). The aerosol surfaces

181   area was calculated based on the size distribution measurement and corrected to wet particle-state by

182   a hygroscopicity growth factor, with a total uncertainty of determining wet aerosol surface areas by

183   ~30% (Liu et al., 2013). VOCs were measured by Proton Transfer Reaction Time-of-Flight Mass

184   Spectrometry (PTR-MS)(Wu et al., 2020; He et al., 2022) and an automated gas chromatograph

185   equipped with mass spectrometry or flame ionization detectors (GC-MS). A commercial instrument

186   (Thermo Electron model 42i) was used to monitor NO_x. O_3 was measured by a commercial

187   instrument using ultraviolet (UV) absorption (Thermo Electron 49i). $PM_{2.5}$ was measured by a

188   Tapered Element Oscillating Microbalance (TEOM, 1400A analyzer). SO_2 and CO were measured

189   by commercial instruments (Thermo Electron 43i and 48i). In addition, the meteorological

190   parameters were available during the measurement. Photolysis frequencies were determined by a

191   spectroradiometer (Bohn et al., 2008). The aerosol liquid water content (ALWC) is calculated from

192   the ISORROPIA-II thermodynamic equilibrium model (Clegg et al., 1998). We used the reverse

193   mode in ISORROPIA-II with the input of water-soluble ions along with ambient temperature (T) and

194   relative humidity (RH). Given the high RH in this campaign, we ran the model by assuming aerosol

195   phase were metastable.

196   **Table 1.** Summary of the information about observed gas and particle parameters during the

197   campaign.

Species	Limit of detection	Methods	Accuracy
N_2O_5	6.0 pptv (3σ, 1 min)	FIGAERO-ToF-CIMS	± 30%
$ClNO_2$	4.3 pptv (3σ, 1 min)	FIGAERO-ToF-CIMS	± 30%
NO	60 pptv (2σ, 1 min)	Chemiluminescence	± 20%
NO_2	0.3 ppbv (2σ, 1 min)	Mo convert	± 20%
O_3	0.5 ppbv (2σ, 1 min)	UV photometry	± 5%
VOCs	0.1 ppbv (5 min)	PTR-ToF-MS	± 30%
VOCs	20-300 pptv (1 h)	GC-FID/MS	± 20%
$PM_{2.5}$	0.1 µg m − 3 (1 min)	TEOM	± 5%
CO	4 ppbv (5 min)	IR photometry	± 5%
SO_2	0.1 ppbv (1 min)	Pulsed UV fluorescence	± 10%
HCHO	25 pptv (2 min)	Hantzsch fluorimetry	± 5%
PNSD	14 nm -700 nm (4 min)	SMPS	± 20%
Aerosol composition	<0.16 µg m^{-3} (30 min)	GAC-IC	± 30%
PM_1 components	0.15 µg m^{-3} (4 min)	HR-ToF-AMS	± 30%
Photolysis frequencies	Varies with species (20 s)	Spectroradiometer	± 10%

198

199   **2.3 Box model setup**

200   A zero-dimensional chemical box model constrained by the field campaign data was applied to

201   simulate the $ClNO_2$ chemistry. The box model was based on the Regional Atmospheric Chemical

202   Mechanism version 2 (RACM2) described in Goliff et al. (2013), and chlorine-related chemical

203   mechanism was added (Wang et al., 2017b; Tan et al., 2017). Briefly, chlorine chemistry was adapted

204   to RACM2 from the modifications to Master Chemical Mechanism (Xue et al., 2015), and the

205   oxidation products from reactions between lumped VOC species and chlorine radicals were adapted

206   from those of OH oxidation from RACM2. $j(ClNO_2)$ was calculated according to the NASA-JPL

207   recommendation based on the work by Ghosh et al. (2012). The impact of O_3 by $ClNO_2$ chemistry

208   was assessed by differing the results of two scenarios with and without the constrains of the observed

209     $ClNO_2$ in the model simulation. For the reaction rate constant of the lumped species with Cl, the

210   fastest value from different species was used to represent the upper limit of the impact of chlorine

211   chemistry. It should be note that the setting will lead to overestimation on the contributions from

212     $ClNO_2$ chemistry. The model was constrained by the observed $ClNO_2$, NOx, O_3, CO, VOCs

213   (assignment to RACM2), photolysis frequencies, ambient temperature, and pressure. The model runs

214   were from 29 September to 17 November, 2019 with most of the measurement data taken accounted

215   for, and with a two-days spin-up. The constant lifetime corresponds to a deposition velocity of 1.2

216   cm s^{-1} with an assumed boundary layer height of 1000 m was used for the input trace gases, and the

217   model-generated species were set to 24 hours lifetime due to the loss caused by the dry deposition

218   (Lu et al., 2012). The input data were averaged and interpolated to 1 hour of resolution.

219   **3. Results and discussions**

220   **3.1 Overview of measurement**

221   Figure 1 shows time series of $ClNO_2$ and relevant trace gases, particles, and meteorological

222   parameters during the measurements. In this campaign, the meteorological condition featured high

223   temperature (24.7 ± 3.8 ^{o}C) and high humidity (62.1% ± 15.6%), low wind speed (1.5 ± 0.8 m s^{-1}),

224   and the dominant air flow were from north and northwest. Compared to those with previously

225   measurements at the same site in January 2017 (Yun et al., 2018b), the temperature was higher and

226   relative humidity was lower during the measurements. The average and maximum concentration of

227   particulate matter ($PM_{2.5}$) was 47.6±19.3 μg m^{-3} and 138 μg m^{-3}, respectively, which is significantly

228   lower than that observed in January 2017, with a maximum up to 400 μg m^{-3}. The dominant air

229   pollutant was O_3 with hourly campaign maximum and the average mean daily maximum 8-hour O_3

230   (MDA8 O_3) of 152.8 ppbv and 75.2 ±20.9 ppbv, respectively. There were 27 days out of 53 days

231   with the hourly maximum of O_3 exceeded the Chinese national air quality standard (200 μg m^{-3},

232   equivalent to 93 ppbv), suggesting severe ozone pollution during the measurement period in PRD

region. NO$_2$ concentration was also elevated with 21.0 ± 10.4 ppbv on campaign average. The concurrent high O$_3$ and NO$_2$ made large nitrate radical production rate occurred with a daily average of 2.5 ± 2.1 ppbv h^{-1} (median, 1.8 ppbv h^{-1}). The campaign maximum NO$_3$ production rate was observed up to 18.6 ppbv h^{-1} in the afternoon at 11th November, 2019. At night, the nitrate radical production rate was 1.8 ± 1.5 ppbv h^{-1} on campaign average (median, 1.4 ppbv h^{-1}). However, high NO$_3$ production rate did not mean high concentrations of NO$_3$, N$_2$O$_5$ and ClNO$_2$ in the atmosphere, as the concentration affected by both their sources and sinks.
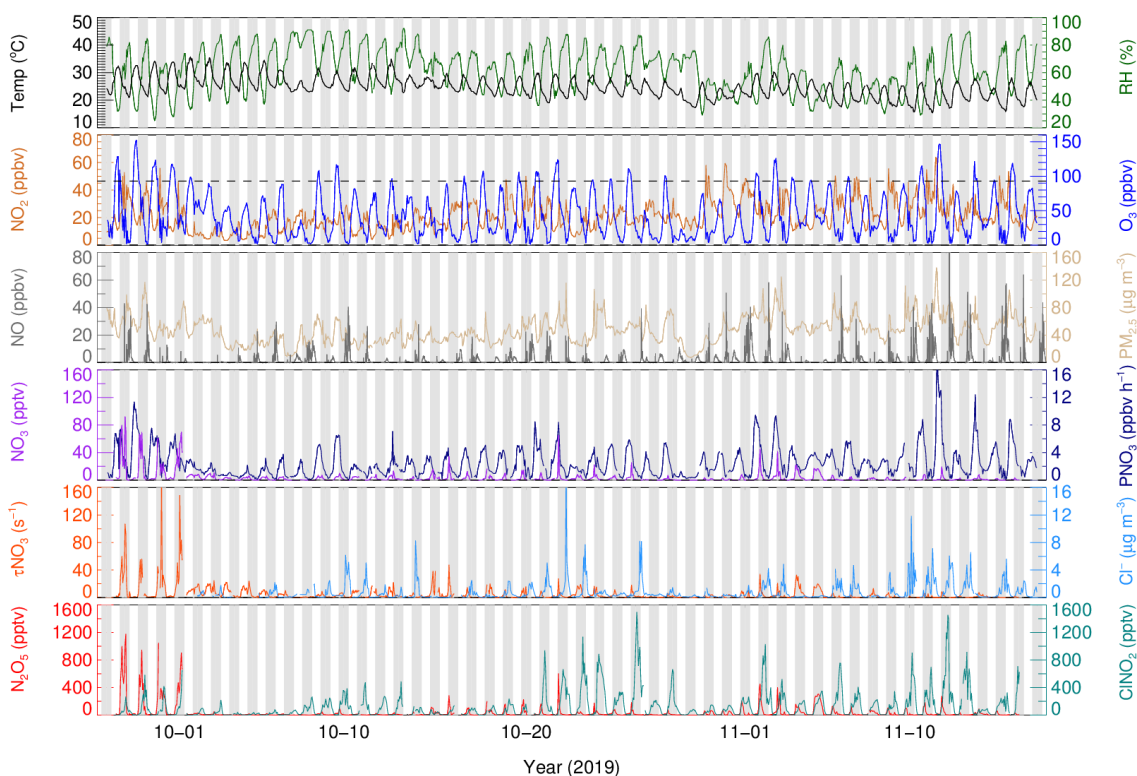
Figure 1. Time series of N$_2$O$_5$, ClNO$_2$ and relevant parameters. The grey dotted line in the O$_3$ panel denotes Chinese national air quality standard for hourly maximum O$_3$ (200 μg m^{-3}, equivalent to 93 ppbv). NO$_3$ radical is calculated based on a thermal equilibrium with measured NO$_2$ and N$_2$O$_5$.

N$_2$O$_5$ existed at a moderate concentration at most nights, with the daily nocturnal peaks range from <100 pptv to 1180 pptv and nocturnal average of 64 ± 145 pptv. During the nights from 27th – 30th September, 2019, the N$_2$O$_5$ concentration was significantly higher than other nights. The NO$_3$ lifetime, calculated by steady state method (Brown et al., 2003), was much longer in the four nights than other nights, implied relative weak sink of NO$_3$-N$_2$O$_5$ for the first four nights. The lifetime of NO$_3$ was < 1 minute in general (except the first four nights), indicating active NO$_3$ chemistry at this site. The NO$_3$ concentration was calculated assuming the thermal equilibrium of NO$_2$-NO$_3$-N$_2$O$_5$, with a possible lower bias caused by the equilibrium coefficient for reversible reactions of NO$_3$ and

252 N$_2$O$_5$ (K_{eq}) (Chen et al., 2022). Figure 1 shows the variation of calculated NO$_3$ coincided with N$_2$O$_5$.

253 Elevated NO$_3$ occurred at the first four nights with a maximum of 90 pptv (1 h time resolution),

254 which is comparable with the reported NO$_3$ level at other sites in Pearl River Delta (Wang and Lu,

255 2019; Brown et al., 2016). ClNO$_2$ showed a clear diurnal variation with high level during the night.

256 The nocturnal average and hourly maximum were 198±232 pptv and 1497 pptv, respectively. The

257 abundance of ClNO$_2$ and N$_2$O$_5$ are lower than those observed at the same site in 2017, with high

258 N$_2$O$_5$ and the highest value ever observed ClNO$_2$ of 3358 pptv and 8324 pptv (1-minute time

259 resolution), respectively (Yun et al., 2018b). The difference of ClNO$_2$ level between the two

260 campaigns conducted in 2017 and 2019 may be caused by the aerosol loading. High particulate

261 chloride ion was observed in the site with 0.74 ± 1.33 μg m^{-3} on nocturnal average, which was higher

262 at night with a peak in the second half of night and decrease at daytime.

263 **3. 2 Characterization of pollutants in different air masses.**

264 We noticed the air mass is highly varied during the measurements. For example, during the period of

265 10/02 - 10/05, the observed ozone and ClNO$_2$ were much lower than other days; while during the

266 period of 11/11 - 11/13, the air masses were much polluted with high O$_3$, PM$_{2.5}$ and ClNO$_2$. We

267 therefore plotted the backward trajectories of 24 h history of air masses arriving at the measurement

268 site at 500 m AMSL height at 00:00, 06:00, 12:00, 18:00 day by day. The measurement period was

269 separated into three patterns meteorologically according to the analysis of backward trajectories.

270 Table 2 listed the detailed information about the air mass classification. The air masses from

271 northeast (and north) were the dominant with a total of 37 days, which was characterized with the

272 outflow of the center city clusters of PRD and those from inland through long distance transport. We

273 checked the pollutants of the air masses from PRD and the north out of PRD (e.g., Hunan or Jiangxi

274 Province), while no significant difference was found. Therefore, we merged the two inland air

275 masses as Type A. The second type was from the coastal or offshore from east and southeast (Type

276 B), which features the outflow of coastal cities like Shenzhen and Hong Kong, which occurred on 12

277 days in total. The third type was the clean air masses from the South China Sea (4 days, Type C).

278 Figure 2 shows three cases of each air masses mentioned above.

279 **Table 2.** The detailed information of three air mass types.

Air mass type	Periods	Days
Type A: inland air from northeast	09/26-10/01;10/08;10/11-10/20;10/24-11/10;11/14-15	37 (69.8%)
Type B: coast air from east	10/06-07; 10/09-10; 10/21-23; 11/11-13; 11/16-17	12 (22.6%)

| Type C: | 10/02-05 | 4 (7.5%) |
| marine air from south | | |

280   The mean diurnal profiles of measured NO_2, O_3, N_2O_5, $ClNO_2$, the particle chloride content and

281   the ratio of chloride to sodium in the three types of air masses are shown in Figure 3, with a detailed

282   summary of related parameters in nocturnal medians listed in Table 3. High levels of NO_2 and O_3

283   were observed in Type A and B air masses, with small difference of NO_2 diurnal variation during the

284   second half of night. In comparison, the two pollutants in Type C were much lower. If we focus on

285   the abundance at night, we found a large difference in NO_2 level with a sequence Type A > Type B >

286   Type C, which results in the same sequence of NO_3 productions in different air masses. The

287   nocturnal NO_2 seems to be a good indicator of the level of pollution, that nocturnal CO, $PM_{2.5}$ and

288   SO_2 also followed this order with highest concentration in Type A. These results indicate that the

289   most polluted air mass came from the inland urban regions of PRD.

290
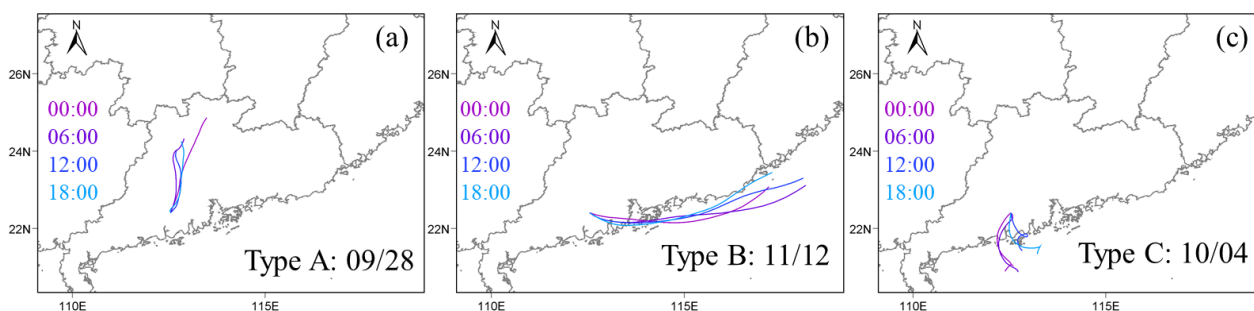
Figure 2. Three typical cases with air mass from different regions at 29th Sept., 12th Nov. and 4th Oct.,

292   respectively. Backward trajectory of 24 h history of air masses arriving at the measurement site with

293   500 m height at 00:00, 06:00, 12:00, 18:00.

294   Given the particulate chloride a precursor of $ClNO_2$, we examined its diurnal variations in the

295   three air mass types. The highest level of Cl^- was found in Type B, and then followed by Type A and

296   Type C (also at night). Although the diurnal profile of Cl^- in the three types is similar, the increasing

297   rate of Cl^- during the second half of night in Type A is much slower than those in coastal and offshore

298   air masses. This imply a difference source of chloride, which will be further discussed in the Section

299   3.4. N_2O_5 was observed with moderate concentration in the Type A air mass throughout the night,

300   with a nocturnal peak of 152.4 pptv between 20:00-21:00, while little N_2O_5 only occurred in the first

301   half of night in Type B and C with a peak of 75.9 pptv and 13.6 pptv, respectively. The concentration

302   difference may be attribute to two aspects. Firstly, the difference of $P(NO_3)$ results in more N_2O_5

303   produced in Type A. Secondly, compared with the air mass from coastal or offshore regions, the

304   nocturnal temperature and RH condition from Type A is much lower, and the loss of N_2O_5 may be

305 faster in Type B and C than that in Type A. The nocturnal median RH in Type A reached up to 67%,

306 while 78% and 79% in Type B and Type C, suggesting a favorable condition for heterogeneous

307 hydrolysis of N_2O_5 for all the three air mass types. The elevated $ClNO_2$ was observed in Type A and

308 B with a nocturnal peak of 273.6 pptv and 479.8 pptv, respectively. Significantly less $ClNO_2$ was

309 observed in Type C air mass with a peak of 82.6 pptv. The reason of the different levels of $ClNO_2$

310 observed in the three air masses types are discussed in Section. 3.4.
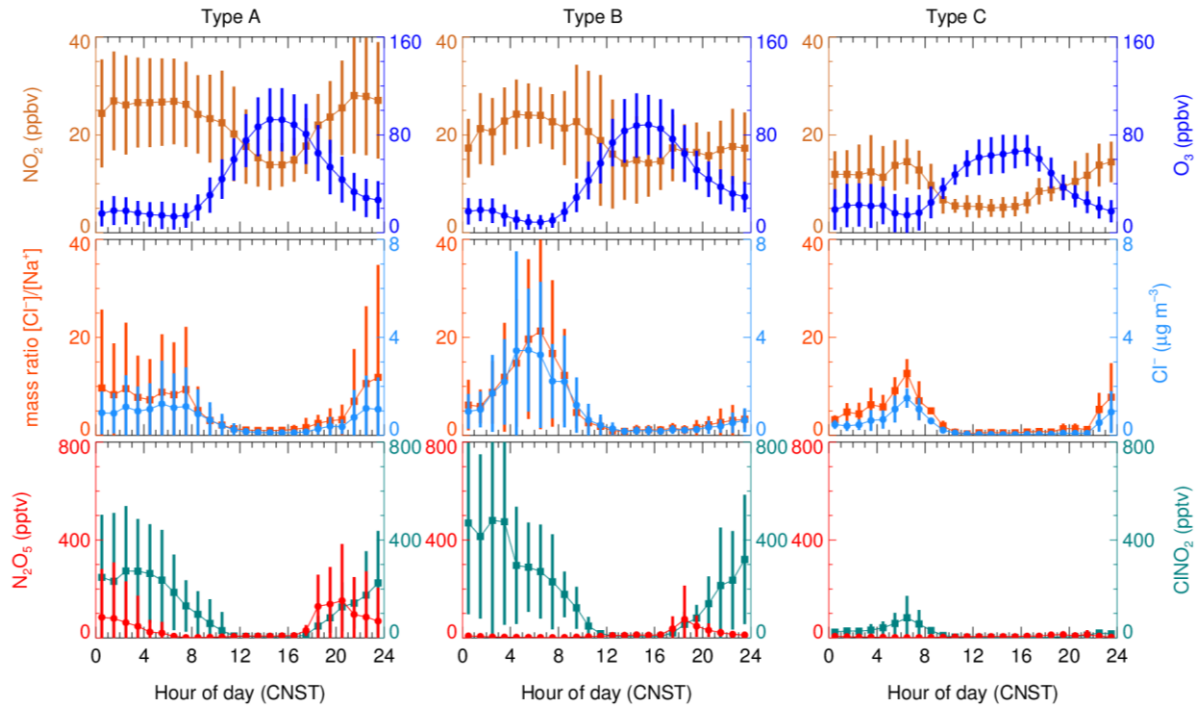
311

312 **Figure 3.** Mean diurnal profiles of N_2O_5, $ClNO_2$ and relevant parameters in the three types of air

313 masses.

314 **Table 3.** Statistics results (median ± standard deviation) of the related parameters in the three types

315 of air masses (from 18:00 to 06:00 CNST).

Air mass	Type-A	Type-B	Type-C
RH (%)	67.0 ± 11.9	78.0 ± 10.9	79.0 ± 9.1
T (°C)	22.8 ± 3.0	23.3 ± 2.2	25.6 ± 1.9
$ClNO_2$ (pptv)	131.0 ± 202.8	162.0 ± 310.1	16.7 ± 21.2
N_2O_5 (pptv)	17.8 ± 164.9	6.3 ± 64.6	2.8 ± 9.3
Cl^- (μg m^{-3})	0.41 ± 1.11	0.56 ± 1.85	0.33 ± 0.51
$PM_{2.5}$ (μg m^{-3})	53.0 ± 18.8	41.0 ± 21.8	32.0 ± 10.2
SO_2 (ppbv)	5.0 ± 4.7	3.4 ± 11.4	3.4 ± 4.7
Na^+ (μg m^{-3})	0.12 ± 0.07	0.18 ± 0.09	0.09 ± 0.03
$P(NO_3)$ (ppbv h^{-1})	1.60 ± 1.49	1.39 ± 1.50	0.69 ± 0.49
NO_2 (ppbv)	24.8 ± 10.9	18.1 ± 6.2	11.2 ± 5.8
O_3 (ppbv)	24.4 ± 21.8	29.5 ± 23.1	22.4 ± 15.2
CO (ppbv)	540.3 ± 122.3	448.4 ± 130.7	367.5 ± 89.8

3.3 N_2O_5 uptake coefficient and $ClNO_2$ yield

In line with previous studies, we estimate N_2O_5 uptake coefficient and $ClNO_2$ yield using the measurements of N_2O_5, $ClNO_2$ and particulate nitrate (Phillips et al., 2016; Wang et al., 2018; Tham et al., 2018). By assuming both the nocturnal enhancement of nitrate and $ClNO_2$ are mainly attributed to N_2O_5 uptake processes, $ClNO_2$ yield can be solely derived by the regression analysis of $ClNO_2$ versus particulate nitrate (Wagner et al., 2012; Riedel et al., 2013). The $\varphi ClNO_2$ can then be obtained by the fitted regression slope (S, Eq. 1) and named as regression method.

$\varphi = 2S/(S+1)$ (Eq. 1)

Combining with the data of N_2O_5 and aerosol surface area, the increase in $ClNO_2$ and nitrate can be simulated simultaneously by setting the input of N_2O_5 uptake coefficient and $ClNO_2$ yield (named as simulation method). The optimal N_2O_5 uptake coefficient and $ClNO_2$ yield are obtained simultaneously by adjusting the two parameters until the simulation reproduces the observed increase $ClNO_2$ and nitrate (Phillips et al., 2016; Xia et al., 2020; Tham et al., 2018). This analysis assumes only N_2O_5 uptake process dominates the increase of $ClNO_2$ and nitrate, and other physicochemical processes like vertical transportation, depositions are less important. This method requests the air mass in the analysis duration time is relative stable and less affected by emission and transportation. In addition, it is not valid in the case with negative changes of $ClNO_2$ and nitrate. The following selection criteria is set to pick out the suitable plumes to meet the assumptions. Firstly, the consistent increase trends of $ClNO_2$ and the NO_3^- and clear correlation between them during the analysis duration should be observed with a regression coefficient threshold of 0.5, which indicates the two products have the same source. Secondary, an equivalent or faster increase of ammonium accompanied with nitrate, to ensure insignificant degas of HNO_3 to the atmosphere. The observational data were averaged to 30 min for the following analysis, the time-period of each derivation ranges from 2.5 to 10 hours. Figure 4 depicts an example of the derivation on 5th November, 2019, the stable Sa indicates stable air mass during the analysis period. And the prediction is well reproduced the observed increase in $ClNO_2$ and NO_3^-.

During this campaign, we carefully identified 20 plumes with clear correlations between $ClNO_2$ and particulate nitrate by the slope method ($R^2 \geq 0.5$). As shown in Table 4, the derived $ClNO_2$ yield varied from 0.13 to 1.00 with a median of 0.45 ± 0.22 (mean value of 0.44). In the 20 plumes, we derived N_2O_5 uptake coefficient and $ClNO_2$ for 12 cases in total. The results in other 8 night were not valid due to the lack of Sa data (four nights) or producing unreasonably high results due to the observed low N_2O_5 concentration near the detection limit biased the simulations. We show good consistent of derived $ClNO_2$ yields by the two different methods. The estimated N_2O_5 uptake coefficient showed a large variation and ranged from 0.0019 to 0.077 with a median of 0.0195 ±

0.0288 (mean value of 0.0317). The estimated γN_2O_5 is within the range determined by previous field studies (Tham et al., 2018). Specifically in China, the average level of γN_2O_5 is comparable with those reported in urban Beijing (Wang et al., 2017a; Wang et al., 2018), Wangdu (Tham et al., 2018), and Jinan (Wang et al., 2017c) during the summertime, but systematically higher than those determined in China in wintertime (Xia et al., 2021; Wang et al., 2020a; Brown et al., 2016), except the case reported on the urban canopy of Beijing (Chen et al., 2020). McDuffie et al. (2018a) summarized the reported $\varphi ClNO_2$ based on the observations, and we showed that the estimated average $\varphi ClNO_2$ in this study is in the middle to upper end of the values reported globally (Xia et al., 2021; McDuffie et al., 2018a). Due to the limited data points, we cannot distinguish the difference of γN_2O_5 between the three air mass patterns. The $ClNO_2$ yields in Type A are slightly lower than those in Type B with an average of 0.41 and 0.47, respectively.
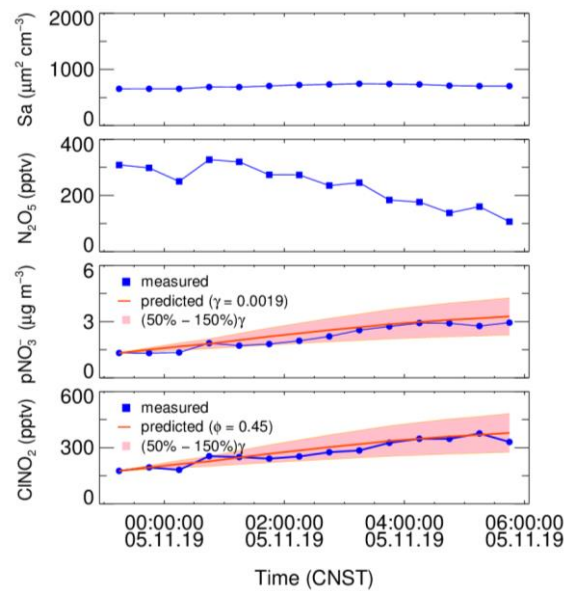
Figure 4. An example of the derivation of N_2O_5 uptake coefficient and $ClNO_2$ yield constrained by observation of aerosol surface area, N_2O_5 and the enhancement of particulate nitrate and $ClNO_2$ on 5th November, 2019. The pink region presents ±50% uncertainty of N_2O_5 uptake coefficient.

Table 4. The derived N_2O_5 uptake coefficient and $ClNO_2$ yields at each night.

NO.	Period	γN_2O_5 [a]	$\varphi ClNO_2$ [a]	$\varphi ClNO_2$ [b]	r^2 [b]	Type
1	10/02 01:00-06:00	NaN	NaN	0.13	0.90	C
2	10/02 23:00-06:00	NaN	NaN	0.25	0.90	C
3	10/11 01:00-04:00	NaN	NaN	0.65	1.00	B
4	10/14 23:00-04:00	0.017	0.28	0.23	0.56	A
5	10/18 18:00-21:00	0.0059	0.42	0.40	0.90	A
6	10/20 20:30-23:00	0.045	0.44	0.47	0.71	A
7	10/21 20:30-01:00	0.061	0.52	0.54	0.90	B

8	10/22 22:30-05:00	0.066	0.58	0.61	0.62	B
9	10/24 22:00-06:00	0.065	0.26	0.23	0.74	A
10	10/25 21:00-02:00	0.077	1.00	1.00	0.92	A
11	10/28 21:00-04:00	NaN	NaN	0.15	0.74	A
12	11/01 21:00-23:30	0.022	0.35	0.32	0.83	A
13	11/02 22:00-00:30	NaN	NaN	0.29	1.00	A
14	11/03 18:00-06:00	0.0031	0.52	0.50	0.92	A
15	11/04 22:00-06:00	0.0019	0.45	0.47	0.86	A
16	11/08 00:00-06:00	0.0097	0.34	0.32	0.85	A
17	11/10 00:00-04:00	NaN	NaN	0.59	0.80	A
18	11/11 22:00-04:00	NaN	NaN	0.53	0.50	B
19	11/12 22:00-04:00	NaN	NaN	0.42	0.62	B
20	11/13 21:00-00:00	0.0070	0.70	0.75	0.92	B

Note: [a] the values of γN_2O_5 and $\varphi ClNO_2$ are derived by simulation method; [b] the $\varphi ClNO_2$ and the correlation coefficient (R^2) between $ClNO_2$ and particulate nitrate are derived by regression method, the data was filtered with a correlation coefficient obtained from linear fitting threshold of 0.5.

To gain insight into the factors governing the N_2O_5 uptake and $ClNO_2$ formation processes, the estimated γN_2O_5 and $\varphi ClNO_2$ were compared with those predicted from complex laboratory-derived and field-derived parameterizations. An aqueous inorganic iconic reaction mechanism once raised by Bertram and Thornton (2009) and established a volume-limited parameterization by considering the aerosol volume, surface area, nitrate content, ALWC, and chloride content (named BT09, Eq. 8).

$$\gamma_{BT09} = \frac{4H_{aq}Vk}{CS_a}\left(1 - \frac{1}{1 + \frac{k_3[H_2O]}{k_{2b}[NO_3^-]} + \frac{k_4[Cl^-]}{k_{2b}[NO_3^-]}}\right) \tag{8}$$

Where H_{aq} is Henry's law coefficient of N_2O_5, V is the aerosol volume; k is equal to $1.15\times10^6 - (1.15\times10^6)^{\exp(-0.13[H2O])}$; k_3/k_{2b} is the ratio of reaction rate of H_2O versus NO_3^- to $H_2ONO_2^+$ that was set to 0.06, and k_4/k_{2b} is the ratio of reaction rate of Cl^- versus NO_3^- to $H_2ONO_2^+$ that was set to 29 (Bertram and Thornton, 2009). The mean values of particulate volume to surface ratio (V/Sa) was measured. A simple parameterization (EJ05) considered the effect of enhanced RH and temperature on N_2O_5 uptake was also included (Evans and Jacob, 2005). In addition, the recently established empirical parameterization based on the same framework (Eq. 8, named Yu20), optimized some parameters according to the meta-analysis of five field measurements in China by Yu et al. (2020), also assessed in the study. Figure 5(a) shows the correlation of estimated γN_2O_5 versus the parameterization. All the three parameterizations fail to predict the high values. The simple parameterization of EJ05 had the best performance with a high correlation and a consistent

prediction of the median value. While other two parameterizations, BT09 and Yu20, underestimated the observed γN_2O_5. Figure 6(a-h) show the dependence of the observed γN_2O_5 on the factors reported in previous literatures that possibly alert the processes of N_2O_5 uptake and $ClNO_2$ formation. We show that γN_2O_5 highly correlated with the ambient RH as well as liquid water content, confirming the critical role of water content in N_2O_5 uptake and explained the reason why EJ05 had a good performance. The dependence of γN_2O_5 on nitrate mass concentration does not follows the rule of nitrate suppressing effect (Wahner et al., 1998), which may be due to the covariance of nitrate and liquid water content. With respect to other factors, insignificant impacts on the N_2O_5 uptake are obtained.
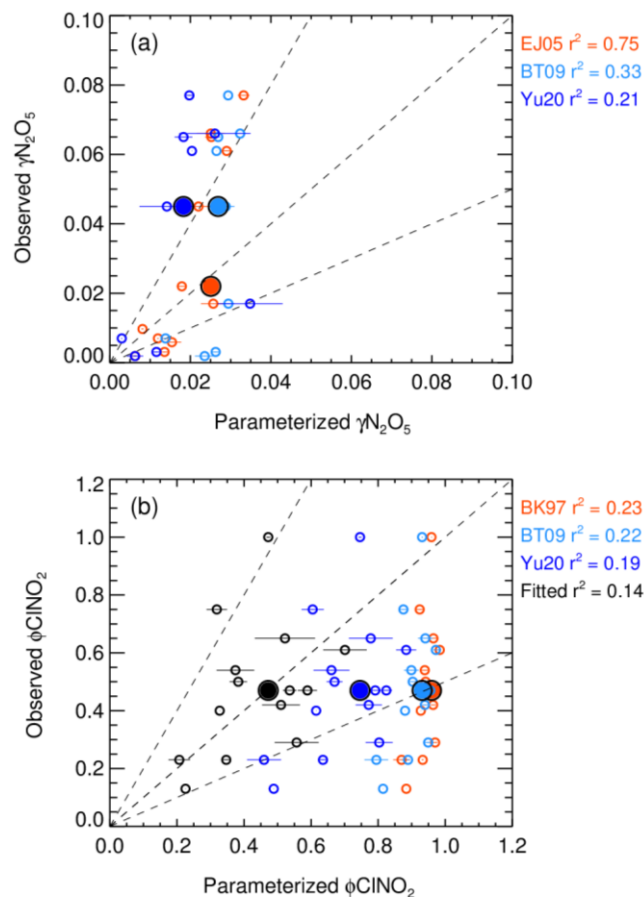
Figure 5. The inter-comparison of observation and parameterization of N_2O_5 uptake coefficient (a) and $ClNO_2$ yield (b). The larger size of solid dots represents the median results. The parametrizations of EJ05, BT09, Yu20 and BK97 cited from Evans and Jacob (2005), Bertram and Thornton (2009), Yu et al. (2020), Behnke et al. (1997), respectively. The fitted $ClNO_2$ yield (colored by black) in panel (b) shows the best fitting result in the study by adopting the k_4/k_3 of 32.0.

Bertram and Thornton (2009) also proposed a $ClNO_2$ yield parameterization method that considering the ratio of ALWC and chloride content (Eq. 9), here the k_4/k_3 was the ratio of reaction

403 rate of $H_2ONO_2^+$ versus Cl^- to H_2O and adopted as 483 ± 175. Behnke et al. (1997) determined this

404 ratio of 836 ± 32, while it is estimated to be 105 ± 37 in Yu et al. (2020).

405 $$\varphi_{BT09} = \left(\frac{[H_2O]}{1+k_4/k_3[Cl^-]}\right)^{-1} \qquad (9)$$

406 Figure 5(b) shows that all the predicting $ClNO_2$ yield based on the abovementioned

407 parameterizations overestimated the observations. The performance of the parameterization schemes

408 of BK97 and BT09 based on the model aerosol conditions with an overestimation up to ~100% are

409 expected and consistent with previous studies, which may be caused by the unaccounted potentially

410 competitive effect of other species like organics, sulfate for the NO_2^+ intermediate (McDuffie et al.,

411 2018a; Staudt et al., 2019; Xia et al., 2021; Wang et al., 2017d). Although the empirical

412 parameterization (Yu20) based on field observations improved the prediction and narrowed the gap

413 effectively, the overestimation is still large with an average of ~50%, which indicated that the yield

414 are more strongly suppressed in this study than those observed in the campaigns of Yu et al. (2020).

415 The factor 32.0 (k_4/k_3 in Eq. 9) was derived by iterative algorithms to achieve the best consistent

416 between the observed and parameterized $ClNO_2$ yield, which is smaller than the Yu20 parameters by

417 factors of 3.3. We examined the relationships of $ClNO_2$ yields with aerosol water content and other

418 aerosol compositions as shown in Figure 6(i-p). We show that $\varphi ClNO_2$ only weakly correlated with

419 the content of chloride (including the mass ratio and fraction in $PM_{2.5}$) and the molar ratio of chloride

420 to water, confirmed the dependence found in laboratory studies. However, we did not find the

421 dependence of the yields with aerosol organic or sulfate, as well as the RH and water alone in the

422 campaign, implying the $ClNO_2$ yield mechanism is much more complicated than the laboratory

423 conditions.
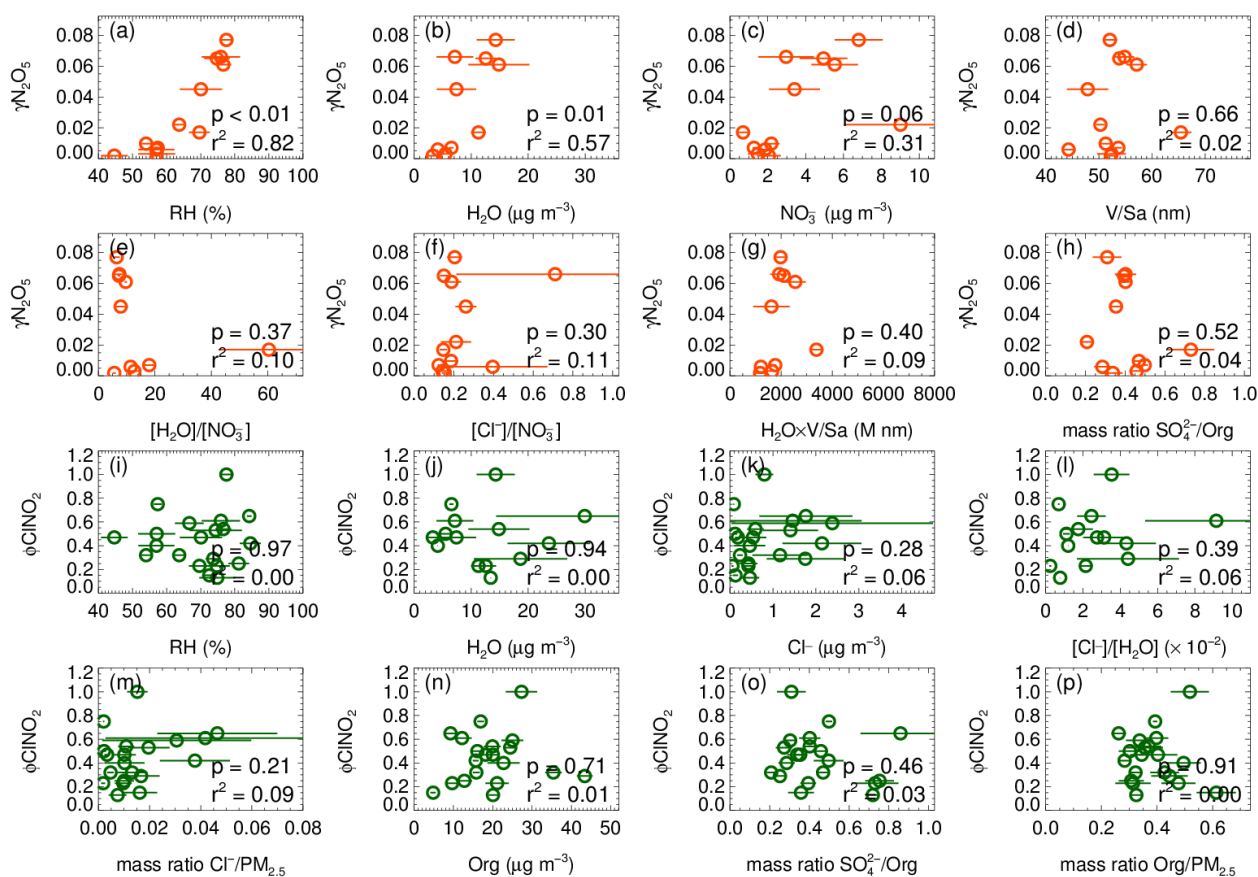
Figure 6. The estimated N_2O_5 uptake coefficient and $ClNO_2$ yield versus related parameters.

3.4 The factors influence $ClNO_2$ formation

The $ClNO_2$ formation can be largely affected by the budget of NO_3-N_2O_5 and N_2O_5 uptake processes. The variation of NO_3 loss by VOC and NO alert the NO_3 loss distribution by N_2O_5 uptake and $ClNO_2$ formation indirectly. Figure 7 shows the correlation between daily median $ClNO_2$ and mass concentration of chloride, $PM_{2.5}$ and NO_3 production rate for the three types of air masses. Due to the limited dataset of type C, the correlation analysis may not make sense, therefore, we did not take type C into consideration in detailed discussion. We show that the mass concentration of chloride also showed a correlation coefficient with $ClNO_2$ by 0.66 and 0.31 for type A and B, respectively. Furthermore, the mass concentration of $PM_{2.5}$ correlated reasonably with the $ClNO_2$ formation with the correlation coefficient of 0.39 and 0.62 for type A and B, respectively. But, the levels of $ClNO_2$ demonstrate little relationship with the nitrate production rate. This is quite different from the results observed in United Kingdom, where the $ClNO_2$ levels are mainly controlled by NO_2 and O_3, rather than by the N_2O_5 uptake processes (Sommariva et al., 2018).
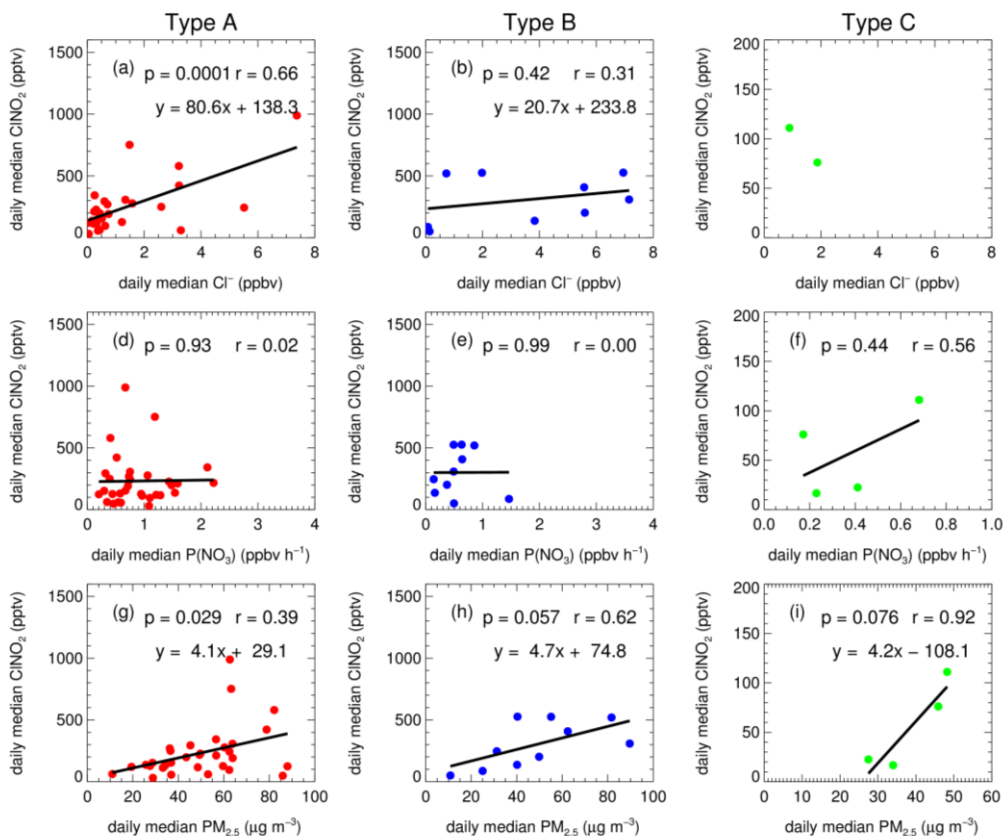
440   **Figure 7.** The functional dependence of daily median of ClNO$_2$ on particulate chloride, nitrate

441   radical production rate and PM$_{2.5}$ in the air mass of Type A (a, d, g), Type B (b, e, h) and Type C (c, f,

442   i).

443   The low correlation between ClNO$_2$ and NO$_3$ production rate is within expectations. In general,

444   the production of nitrate radical controls the total budget of N$_2$O$_5$, if N$_2$O$_5$ uptake dominated the sink

445   of NO$_3$, as the result the N$_2$O$_5$ uptake and its products would show good correlation with NO$_3$

446   production rate. But in fact, NO$_3$ loss can also be affected by other loss pathways, like the reactions

447   with NO and VOCs. In many cases, the NO$_3$ loss is dominated by VOC or NO, that means the

448   ClNO$_2$ formation is suppressed. If the two loss pathways are highly varied due to irregular emissions,

449   then the relationship between ClNO$_2$ and NO$_3$ production rate would be less correlated. We

450   confirmed large variations of NO and VOC (not shown) in hourly and daily scales, which means the

451   proportion of N$_2$O$_5$ uptake to the total loss of NO$_3$ is highly varied correspondingly. In addition, the

452   variation of N$_2$O$_5$ uptake coefficient and ClNO$_2$ yield also result in the weak correlation between

453   NO$_3$ production rate and ClNO$_2$ concentration. The weak correlation reflects the highly variable

454   chemical processes from NO$_3$ production to ClNO$_2$ production in this region.

455   As the precursor of ClNO$_2$, higher concentrations of particulate chloride result in high ClNO$_2$

456   yield from N$_2$O$_5$ uptake to some extent, as evidenced by our field observation (Figure 6) and

457   previous laboratory studies (Bertram and Thornton, 2009; Roberts et al., 2009; Ryder et al., 2015).

458   High $PM_{2.5}$ concentrations usually provide more aerosol surface area to promote N_2O_5 uptake. The

459   close relationship between $ClNO_2$ and $PM_{2.5}$ indicate that aerosol surface area, most likely, is a

460   critical factor that limited $ClNO_2$ formation. The proportion of nitrate in the total $PM_{1.0}$ was small

461   with an average of 10.4%, therefore the correlation of $ClNO_2$ and $PM_{2.5}$ cannot attribute to the

462   covariance between nitrate and $PM_{2.5}$. In addition, the $ClNO_2$ level in the air mass of Type B show

463   higher correlation to both Cl^- and $PM_{2.5}$ than type A, suggesting that the $ClNO_2$ formation in Type B

464   is more effectively affected by the levels of chloride and $PM_{2.5}$.

465   Recently model simulation indicated that the $ClNO_2$ chemistry level is sensitive to the emission of

466   chloride in PRD (Li et al., 2021). In this study, a question raised that where is the source of chloride?

467   The mass ratio of Cl^-/Na^+ is often used as an indicator of sea salt or anthropogenic sources to

468   chloride with a threshold of 1.81 (Yang et al., 2018; Wang et al., 2016). High ratio means the

469   particulate chloride affected by anthropogenic emission rather than sea salt. We determine that the

470   mean mass ratios of Cl^- to Na^+ are 5.3, 6.3 and 3.1 in Type A, B and C, respectively (Figure 3). This

471   indicated that $PM_{2.5}$ sampled during the campaign was not strongly influenced by fresh sea salt

472   aerosols. In the three types, the Type C air mass had a lowest ratio and may be influenced by both sea

473   salt and anthropogenic emissions, which seems reasonable since it come from South China Sea. If

474   we assume that Type A air mass is free of sea salt and only influenced by anthropogenic activities,

475   the higher ratio implies more intensive chloride source in Type B. The correlation between

476   particulate chloride and some possible indicators, including K^+, benzene, SO_2, CO, acetonitrile

477   (CH_3CN), were examined day by day. Figure 8 shows the max correlation coefficient (R^2) in each

478   day with a threshold of 0.5. We filtered out 39 out of 46 days during this campaign with a fraction of

479   85%. Among the 39 days, a total of 11 days is associated with strongest correlation between Cl^- and

480   benzene, which is typically come from industrial emissions. Cl^- also correlated with K^+, CO and

481   CH_3CN in 19 day in total, implies potential contributions from biomass burning emissions. In total of

482   9 days for highest correlations of Cl^- with SO_2 indicated coal-fired power plants emissions may also

483   contributed to Cl^- emission. We summarized that the source of chloride may be highly varied from

484   different anthropogenic activities including biomass burning, industrial processes as well as coal-

485   fired power plants. The statistic results in Table 5 suggest that the Cl^- in air mass of Type A were

486   affected by various sources, especially related to the sources associated with K^+, benzene and

487   CH_3CN; the Cl^- in Type B was mainly contributed by the similar source of CO, and Type C was only

488   affected by coal-fired power plants emissions. In addition, Figure 8 showed that there are 2 days that

489   the correlations between Cl^- and Na^+ exceeded the max of the selected anthropogenic factor matrix,

490   indicated that the aerosol still also impacted by sea salt to some extent.

491
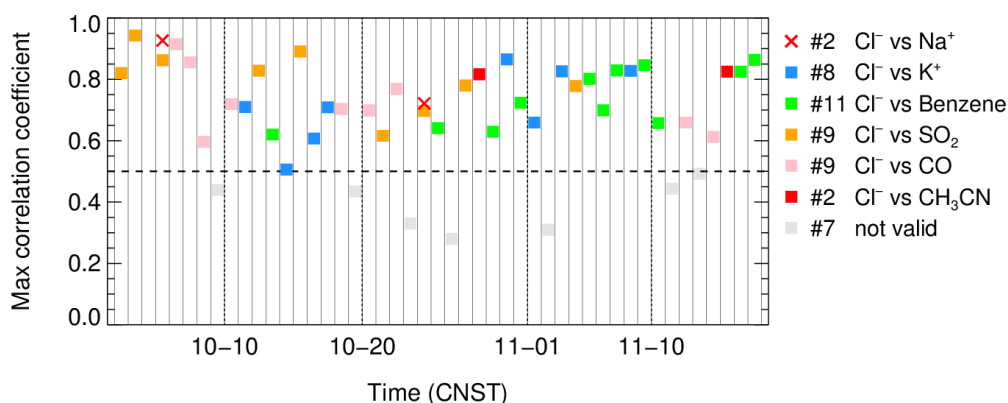
Figure 8. The max correlation coefficient between particulate chloride and a selected parameter matrix (including K^+, benzene, SO_2, CO, acetonitrile (CH_3CN)) in each day. The labelled number in each legend indicates the days be the maximum, the dashed line denotes the threshold of 0.5 (39 valid days out of 46 in total). The cross means the correlation coefficient between Cl^- and Na^+ is larger than the max.

Table 5. The statistic of the days for highest factors correlated with particulate chloride in different air mass pattern.

Factors	Type A	Type B	Type C
K^+	8	0	0
Benzene	9	2	0
SO_2	5	1	3
CO	4	5	0
CH_3CN	2	0	0

3.5 The impacts of $ClNO_2$ on atmospheric oxidation

In this section, we focus on the assessment of the impact of $ClNO_2$ photolysis on the source of radicals and the contribution to the atmospheric oxidation. Figure 9 shows the diurnal accumulation of ROx production rate from model simulations with $ClNO_2$ chemistry in the three types of air mass. The total ROx production rate was higher in Type A and then followed by Type B and C, in which photolysis of HONO, HCHO, O_3 and OVOCs had large contributions. In addition, we noticed that the significant role of OVOCs (including photolysis and react with O_3) in producing ROx at this site, especially in the Type A and B air mass. This result is consistent with that constrained by observed OVOCs in Guangzhou City (Wang et al., 2022c). Cl radical, liberated by $ClNO_2$, enhanced little ROx production, with a morning peak contribution of 1.3%, 2.2% and 1.8% for Type A, B, C, respectively (08:00-09:00). The contribution of $ClNO_2$ photolysis to the production of ROx is less than 1% on daytime average, similar to the results obtained in winter Shanghai (Lou et al., 2022) as well as North China (Xia et al., 2021), and much lower compared to previous studies reported in summer

512   time in China (Tan et al., 2017; Tham et al., 2016). However, another winter campaign conducted in

513   Hongkong in winter showed much more significant impacts compared with our observation(Wang et

514   al., 2016), indicated that the $ClNO_2$ chemistry can also had a large influence on the radical formation

515   in wintertime.
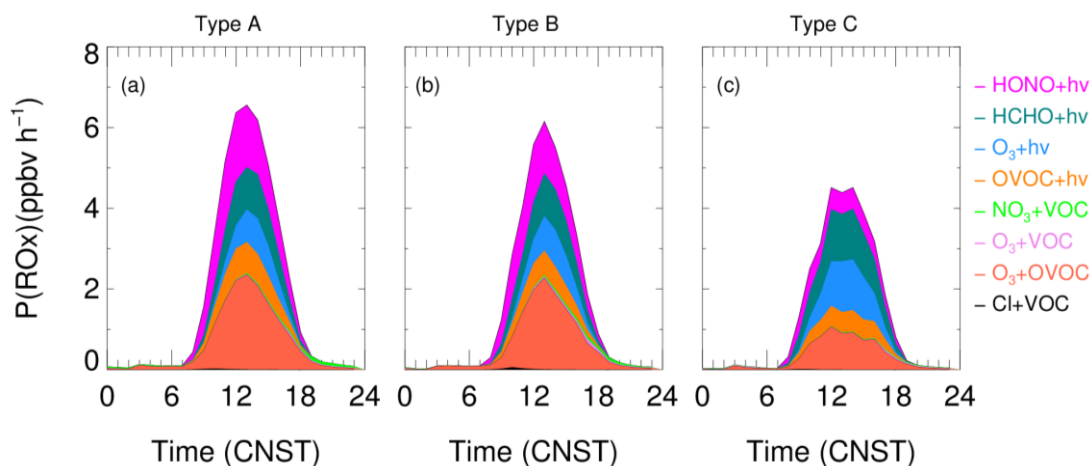
516

517   **Figure 9.** The diurnal cycle and distribution of ROx production rate in the three types air masses.

518   Figure 10 shows the enhancement of OH, HO_2 and RO_2 radicals with the consideration of $ClNO_2$

519   chemistry. The enhancement of the three radicals peaked in the morning. On average, OH

520   concentration was enhanced by 1.5% to 2.6% in different air masses. The percentage of enhancement

521   for HO_2 radical was 1.9% to 4.6%, whereas the enhancement for RO_2 was a little bit higher (3.0% to

522   6.8%). In general, the enhancement of radicals was more significant in Type B than other two types

523   of air masses, which is related to elevated $ClNO_2$ concentrations for these air masses. Low $ClNO_2$

524   and other radical precursors led to an earlier enhancement peak (08:00-09:00) in Type C and lasted a

525   short time period. Although the increase peak occurred later at 09:00-10:00 for the air mass of Type

526   A and Type B, the increase lasted for a longer time and had a longer effect. Overall, daytime OH,

527   HO_2 and RO_2 enhanced by 1.0%, 2.0%, and 3.0% on campaign average.

528
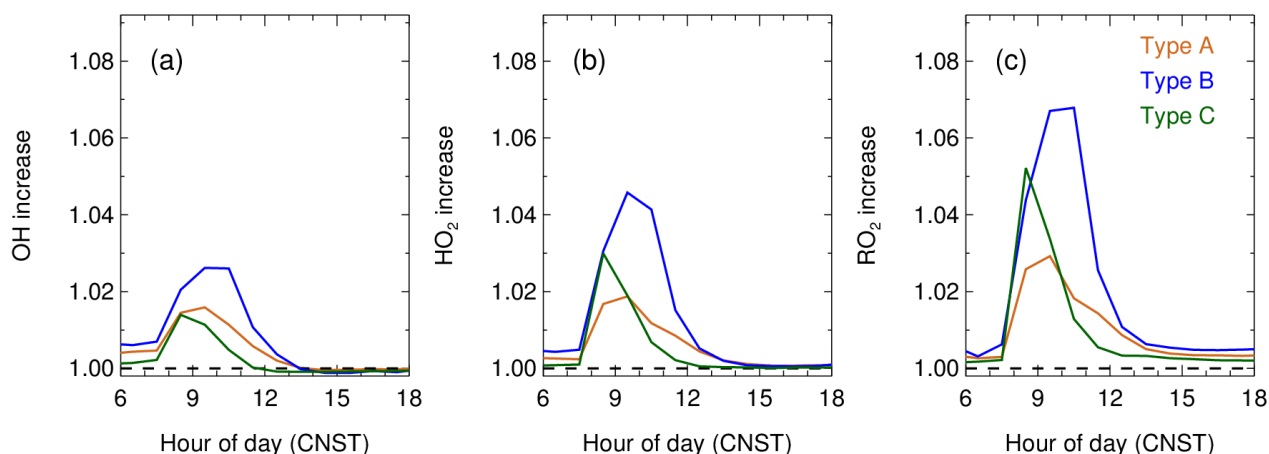
Figure 10. The diurnal cycle on the enhancement of OH (a), HO_2 (b), RO_2 (c) by $ClNO_2$ chemistry in the three air mass patterns.

Figure 11 depicts the integral enhancement of O_3 production by $ClNO_2$ photolysis varied from less than 0.1 ppb to 4 ppb day by day, with a percentage of <1% to 4.9% with a median of 0.8%. Our results are comparable with the winter case in North China (Xia et al., 2021). The next day O_3 enhancement was highly correlated with the level of $ClNO_2$ with the correlation coefficient of 0.7 (Fig. 11(a)). The daily net O_3 production enhanced by 0.70 ppbv (0.9%), 1.02 ppbv (1.9%), 0.24 ppbv (0.6%) on daytime accumulation in Type A, B, C, respectively, which is consistent with the nocturnal level of $ClNO_2$ in the three air masses presented in Table 3.

538
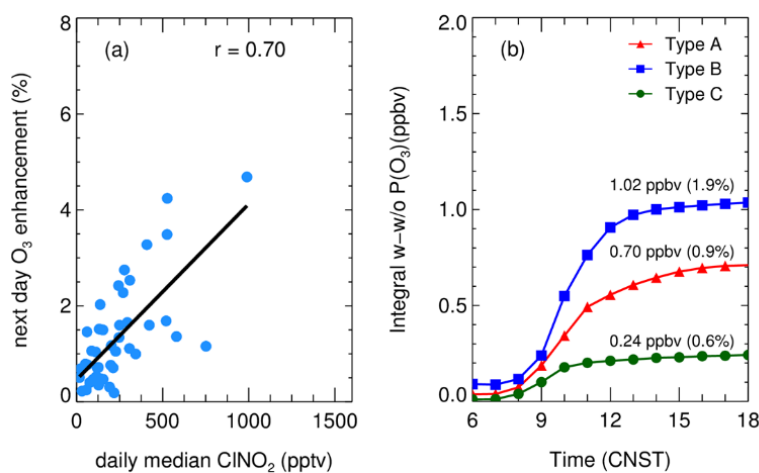
Figure 11. (a) The correlation of daily median $ClNO_2$ (18:00-06:00) and its impact on next day net O_3 production enhancement during the campaign; (b) the average contribution of daytime integral O_3 by $ClNO_2$ mechanism in the three types of air masses.

Table 6 summarized the observation-constrained box model simulation results about the impacts of $ClNO_2$ chemistry. The average $ClNO_2$ concentration in the observation is moderate compared with

previous observations, other radical precursors (e.g., HCHO) also elevated at the same time. This leads to a large total radical and ozone production rate and relative minor contribution by $ClNO_2$ chemistry. Which indicates that the contribution of $ClNO_2$ chemistry is affected by the budget of other radical precursors. In addition, significant contribution by $ClNO_2$ chemistry to photochemical pollution also frequently observed in different campaigns (Tham et al., 2016; Wang et al., 2016), in which the receptor site may have aging plumes with higher $ClNO_2$ and thus larger contributions (Wang et al., 2016), suggests the large variability of $ClNO_2$ and its environmental impacts at various air masses. Here, our observations should be representative of the local condition and reflects the chemistry and impacts of $ClNO_2$ on the air pollutions in PRD region.

Table 6. The summary of impacts of $ClNO_2$ on the next-day enhancement of ozone and radical production based on box model that constrained by field observations in previous literatures.

Location	Duration	$ClNO_2$ peak (ppb)	Daytime average Enhancement $P(O_3)$	Daytime average Enhancement $P(RO_x)$	References
Heshan, CN	2019. 11	1.5	1.0%-4.9%	<2.2%	this work
Shanghai, CN	2020.10-11	0.4	-	<1.0%	Lou et al., 2022
Wangdu/Beijing/ Mt. Tai, CN	2017-2018	1.7	1.3%-6.2%	1.3%-3.8%	Xia et al., 2021
Wangdu, CN	2014.6-7	2.1	3.0%	<10.0%	Tham et al., 2016
Seoul, Korea	2016.5-6	2.5	1.0-2.0%	-	Jeong et al., 2019
Hongkong, CN	2013.11-12	4.7	11.0-41.0%[a]	-	Wang et al., 2016
California, US	2010.5-6	1.5	15.0%[b]	17.0%	Riedel et al., 2014

Note: [a] used box model to estimate the following evolution after the plume passing measurement site and the impacts on the next day air quality; [b] not constrained the observed $ClNO_2$ concentration but simulated the observed maximum $ClNO_2$ case (1.5 ppbv $ClNO_2$) to predict the corresponding upper contribution.

Previous studies suggest that chlorine radicals from $ClNO_2$ photolysis may contribute significantly to the oxidation of some VOCs species, especially for long-chain alkanes(Shi et al., 2020; Wang et al., 2022b). The oxidation of long-chain alkanes (C10~14 n-alkanes) by chlorine and OH radicals during the morning hour (09:00-10:00) were also evaluated based on modeled oxidants concentration. We observe small contributions of chlorine radical with a percentage of 4.3%, 4.3% and 3.8% for n-decane, n-dodecane, and n-tetradecane, respectively, during the period (Oct. 16th to Nov. 17th, 2019) when the long-chain alkanes measurement was valid. We also checked the role of chlorine radicals in short-chain alkanes oxidation, obtaining a slightly larger contribution than the long-chain alkanes, which is attributed to a relatively larger reaction rate constants between Cl with OH with respect to

568   the short-chain alkanes. The daytime average contributions of Cl ranged from 1.4% - 1.6% varied by

569   the chain length of the alkanes. Therefore, we concluded that chlorine radicals liberated by $ClNO_2$

570   photolysis play a role in the oxidation of alkanes in the morning time, but are not critical compared

571   with OH oxidation on the daytime average. We note that several studies reported other sources

572   produced a large number of halogen radicals like Cl_2 (Liu et al., 2017; Xia et al., 2020), BrCl (Peng

573   et al., 2021), the daytime reaction of HCl with OH (Riedel et al., 2012; Eger et al., 2019; Li et al.,

574   2019). These may cause more alkanes oxidized by halogen radicals. However, it is not possible to

575   assess the overall impacts by constraining all precursors of chlorine radical in this work, which may

576   warrant further investigation by more comprehensive field studies equipped with the instruments for

577   detecting these species.

578   **4. Conclusion**

579   An intensive field study in Pearl River Delta took place during a photochemical pollution season

580   from Sept. 26th to Nov. 17th, 2019, providing a comprehensive observation dataset to understand the

581   $ClNO_2$ chemistry and its impacts on the air quality. We observed a wide variation for determining

582   factors of $ClNO_2$ formation in different kinds of air masses. Two types of air mass from northern and

583   northeastern inland cities and the eastern coastal regions, features polluted with elevated O_3 and

584   related trace gases like NOx and CO. Correlation analysis showed that $ClNO_2$ formation is limited by

585   chloride availability and $PM_{2.5}$ concentrations (mostly due to aerosol surface area) at this site.

586   We estimated the N_2O_5 uptake coefficients and $ClNO_2$ yield during this campaign and assessed the

587   performance of previous parameterizations schemes. The newly developed observation-based

588   empirical parameterization was also checked and showed an overall underestimation. We showed the

589   γN_2O_5 only strongly correlated with RH, and the parameterization proposed by Evans and Jacob

590   (2005) showed a considerable consistent with the observation. The $ClNO_2$ yield only showed weak

591   correlation with the content of particle chloride, and the exist parameterizations systematically

592   overestimated the yield. The particulate chloride mainly originated from anthropogenic emissions

593   rather than sea salt. However, the specific contributing source of chloride in this region cannot be

594   determined, due to the varying correlation relationship with different kinds of anthropogenic

595   emission indicators day by day. This result highlights the $ClNO_2$ chemistry may be triggered by

596   many kinds of anthropogenic activities in the PRD regions (Wang et al., 2016; Yang et al., 2018).

597   Observation-constrained box model revealed chlorine radicals liberated by $ClNO_2$ chemistry had a

598   relatively small contribution to the following daytime level of RO_x radicals and O_3 in this region. The

599   small contribution of $ClNO_2$ chemistry in PRD region may be due to the limited $ClNO_2$ produced by

600   N_2O_5 uptake processes, and other strong primary sources of radicals weakened its contribution

601 indirectly. Given complex source of particulate chloride, we call for more field investigations to
602 address the chlorine chemistry and its roles in air pollutions in China.

603 **Data availability.** The datasets and code used in this study are available from the corresponding
604 author upon request (byuan@jnu.edu.cn).

605 **Author contributions.** H.C.W. and B.Y. designed the study. E.Z, X.X.Z. and H.C.W. operated and
606 calibrated the CIMS, H.C.W. analyzed the data, H.C.W. and B.Y. wrote the manuscript with inputs
607 from all coauthors.

608 **Competing interests.** The authors declare that they have no conflicts of interest.

609 *Acknowledgements*. This work was supported by the National Natural Science Foundation of China
610 (grant No. 41877302, 42175111, 42121004), Guangdong Natural Science Funds for Distinguished
611 Young Scholar (grant No. 2018B030306037), Key-Area Research and Development Program of
612 Guangdong Province (grant No. 2019B110206001), and Guangdong Innovative and Entrepreneurial
613 Research Team Program (grant No. 2016ZT06N263). This work was also supported by Special Fund
614 Project for Science and Technology Innovation Strategy of Guangdong Province (Grant
615 No.2019B121205004). The authors gratefully acknowledge the Jinan University science team for
616 their technical support and discussions during this campaign. We thank for the NOAA Air Resources
617 Laboratory for providing the HYSPLIT model.

618 **Appendix**

619 **A1. The measurement background and calibration of CIMS**

620 The background measurement of $ClNO_2$ and N_2O_5 was performed during the campaign. Figure 1A
621 showed an example of the background check at the beginning of the campaign, which confirmed the
622 negligible background signal in the measurement of $ClNO_2$ and N_2O_5 in the ambient condition. The
623 calibration of $ClNO_2$ measurement sensitivity has been introduced in Wang et al. (2022a). In brief, a
624 nitrogen flow (6 mL min^{-1}) containing 10 ppmv Cl_2 was passed over a slurry containing $NaNO_2$ and
625 NaCl to produce $ClNO_2$ (Thaler et al., 2011), and NaCl was included in the slurry in order to
626 minimize the formation of NO_2 as a byproduct. The mixed flow containing $ClNO_2$ was then

627 conditioned to a given RH and sampled into the CIMS instrument. To quantify $ClNO_2$, the mixed

628 flow was delivered directly into a cavity attenuated phase shift spectroscopy instrument (CAPS,

629 Model N500, Teledyne API) to measure background NO_2 concentrations or through a thermal

630 dissociation tube at 365 °C to fully decompose $ClNO_2$ to NO_2, and the total NO_2 concentrations were

631 then determined using CAPS. The differences in the measured NO_2 concentrations with and without

632 thermal dissociation was equivalent to $ClNO_2$ concentrations. The CAPS instrument had a detection

633 limit of 0.2 ppbv in 1 min for NO_2 and an uncertainty of ~10%. To calibrate CIMS measurements of

634 N_2O_5, a humidity adjustable mixed flow containing stable N_2O_5, which was produced via O_3

635 oxidation of NO_2, was sampled into the CIMS instrument to obtain a normalized humidity

636 dependence curve of N_2O_5. While the concentration of N_2O_5 source is not quantified due to the

637 absence of a N_2O_5 detector, so we delivered the N_2O_5 source flow through a supersaturated sodium

638 chloride solution to convert N_2O_5 to $ClNO_2$ with a unit efficiency at 50% RH, which is a widely used

639 method for the calibration of $ClNO_2$ by CIMS technique. The absolute N_2O_5 sensitivity at 50% RH

640 can be realized and then scaled to other humidity condition by the normalized N_2O_5 sensitivity curve

641 determined before. The sensitivity curves for N_2O_5 and $ClNO_2$ to water content were shown in

642 Figure A2. In this study, the sensitivity of the instrument was calibrated after the campaign. The main

643 parameters (pressure: voltages, etc.) of the CIMS were checked every day and were relatively stable,

644 indicating that the CIMS is operating stably during the campaign.

645 Figure A3 shows the high-resolution peak fitting results of typical mass spectra at m/z 235 and m/z

646 208 for N_2O_5 and $ClNO_2$ in three air mass patterns, respectively. The peaks of N_2O_5 and $ClNO_2$ were

647 clearly resolved in the mass spectra. The peak of $IN_2O_5^-$ can be well retrieved by separating a large

648 adjacent peak of $C_2H_4IO_3S^-$ in the air masses affected by marine emissions (Type B and C), which

649 might be hydroperoxymethyl thioformate (HPMTF) from dimethyl sulfide oxidation (Veres et al.,

650 2020). The interference signals including $H_3INO_2S^-$ for $ClNO_2$ measurements can also be well

651 separated in all the three air mass patterns. These results underline the necessity and feasibility in the

652 application of ToF analyzer in detecting N_2O_5 and $ClNO_2$ with iodide CIMS.
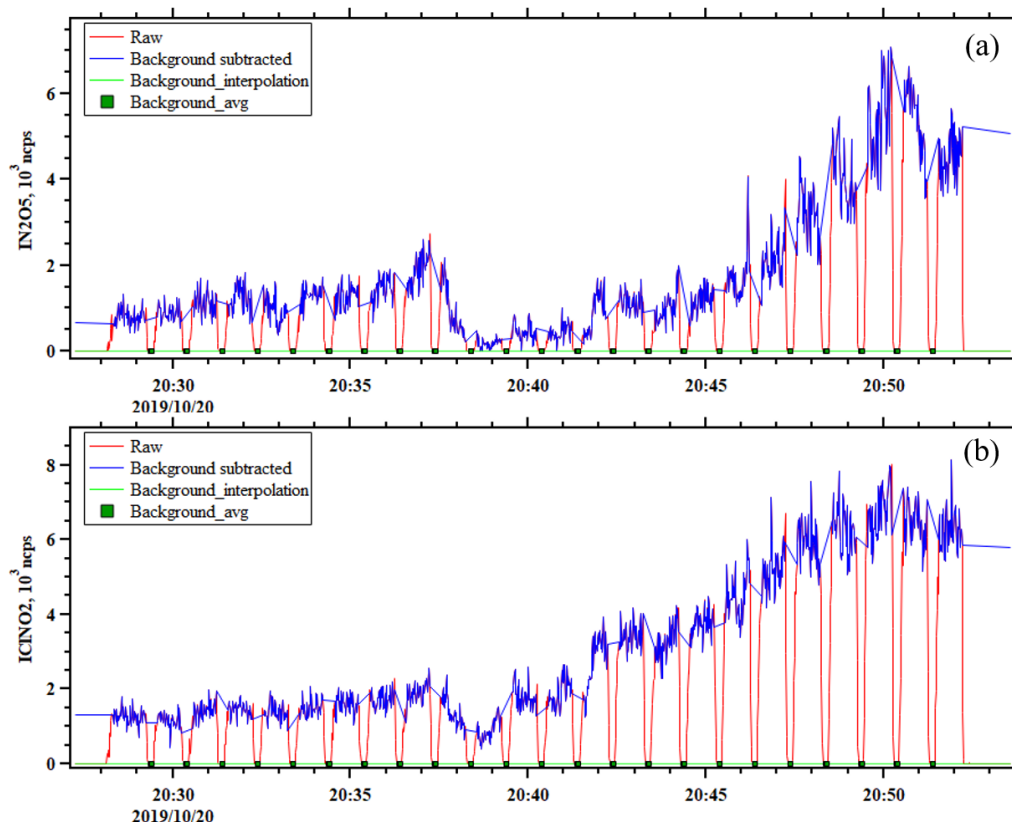
653

654 **Figure A1.** An example of background measurement for N_2O_5 (a) and $ClNO_2$ (b) in October 20th,

655 2019.
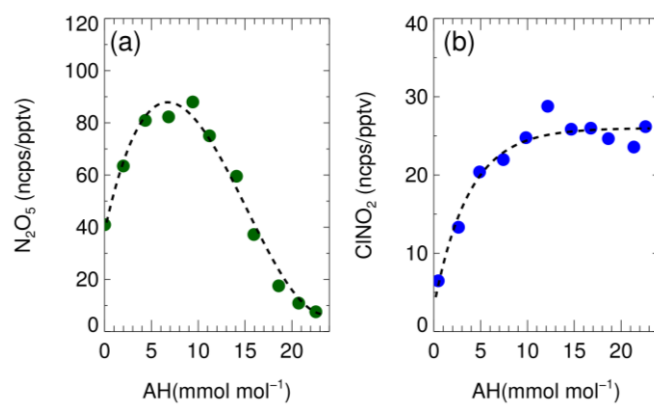
656

657 **Figure A2.** CIMS sensitivities as a function of absolute humidity (AH) for (a) N_2O_5 and (b) $ClNO_2$.
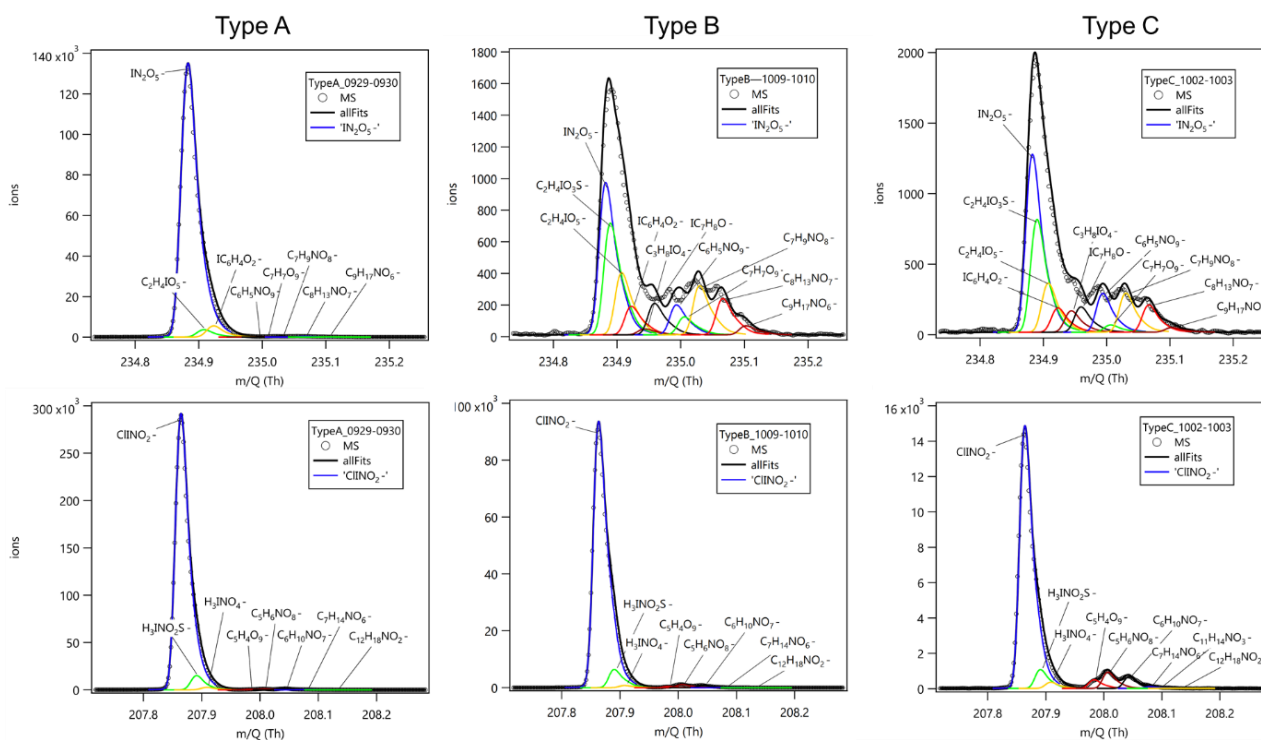
Figure A3. Cases of high-resolution spectra fitting for N_2O_5 and $ClNO_2$ by ToF-CIMS under three air mass patterns.

Reference

Anttila, T., Kiendler-Scharr, A., Tillmann, R., and Mentel, T. F.: On the reactive uptake of gaseous compounds by organic-coated aqueous aerosols: Theoretical analysis and application to the heterogeneous hydrolysis of N2O5, J Phys Chem A, 110, 10435-10443, Doi 10.1021/Jp062403c, 2006.

Atkinson, R., and Arey, J.: Atmospheric degradation of volatile organic compounds, Chem Rev, 103, 4605-4638, 10.1021/cr0206420, 2003.

Atkinson, R., Baulch, D. L., Cox, R. A., Crowley, J. N., Hampson, R. F., Hynes, R. G., Jenkin, M. E., Rossi, M. J., and Troe, J.: Evaluated kinetic and photochemical data for atmospheric chemistry: Volume II - gas phase reactions of organic species, Atmospheric Chemistry and Physics, 6, 3625-4055, DOI 10.5194/acp-6-3625-2006, 2006.

Bannan, T. J., Booth, A. M., Bacak, A., Muller, J. B. A., Leather, K. E., Le Breton, M., Jones, B., Young, D., Coe, H., Allan, J., Visser, S., Slowik, J. G., Furger, M., Prevot, A. S. H., Lee, J., Dunmore, R. E., Hopkins, J. R., Hamilton, J. F., Lewis, A. C., Whalley, L. K., Sharp, T., Stone, D., Heard, D. E., Fleming, Z. L., Leigh, R., Shallcross, D. E., and Percival, C. J.: The first UK measurements of nitryl chloride using a chemical ionization mass spectrometer in central London in the summer of 2012, and an investigation of the role of Cl atom oxidation, Journal of Geophysical Research-Atmospheres, 120, 5638-5657, 10.1002/2014jd022629, 2015.

Bannan, T. J., Bacak, A., Le Breton, M., Flynn, M., Ouyang, B., McLeod, M., Jones, R., Malkin, T. L., Whalley, L. K., Heard, D. E., Bandy, B., Khan, M. A. H., Shallcross, D. E., and Percival, C. J.:

Ground and Airborne UK Measurements of Nitryl Chloride: An Investigation of the Role of Cl Atom Oxidation at Weybourne Atmospheric Observatory, Journal of Geophysical Research-Atmospheres, 122, 11154-11165, 10.1002/2017jd026624, 2017.

Bannan, T. J., Khan, M. A. H., Le Breton, M., Priestley, M., Worrall, S. D., Bacak, A., Marsden, N. A., Lowe, D., Pitt, J., Shallcross, D. E., and Percival, C. J.: A Large Source of Atomic Chlorine From ClNO2 Photolysis at a UK Landfill Site, Geophysical Research Letters, 46, 8508-8516, 10.1029/2019gl083764, 2019.

Behnke, W., George, C., Scheer, V., and Zetzsch, C.: Production and decay of ClNO2, from the reaction of gaseous N2O5 with NaCl solution: Bulk and aerosol experiments, Journal of Geophysical Research-Atmospheres, 102, 3795-3804, Doi 10.1029/96jd03057, 1997.

Bertram, T. H., and Thornton, J. A.: Toward a general parameterization of N2O5 reactivity on aqueous particles: the competing effects of particle liquid water, nitrate and chloride, Atmospheric Chemistry and Physics, 9, 8351-8363, 2009.

Bohn, B., Corlett, G. K., Gillmann, M., Sanghavi, S., Stange, G., Tensing, E., Vrekoussis, M., Bloss, W. J., Clapp, L. J., Kortner, M., Dorn, H. P., Monks, P. S., Platt, U., Plass-Dulmer, C., Mihalopoulos, N., Heard, D. E., Clemitshaw, K. C., Meixner, F. X., Prevot, A. S. H., and Schmitt, R.: Photolysis frequency measurement techniques: results of a comparison within the ACCENT project, Atmospheric Chemistry and Physics, 8, 5373-5391, 2008.

Brown, S. S., Stark, H., and Ravishankara, A. R.: Applicability of the steady state approximation to the interpretation of atmospheric observations of NO3 and N2O5, Journal of Geophysical Research-Atmospheres, 108, Artn 4539
Doi 10.1029/2003jd003407, 2003.

Brown, S. S., Ryerson, T. B., Wollny, A. G., Brock, C. A., Peltier, R., Sullivan, A. P., Weber, R. J., Dube, W. P., Trainer, M., Meagher, J. F., Fehsenfeld, F. C., and Ravishankara, A. R.: Variability in nocturnal nitrogen oxide processing and its role in regional air quality, Science, 311, 67-70, DOI 10.1126/science.1120120, 2006.

Brown, S. S., and Stutz, J.: Nighttime radical observations and chemistry, Chem Soc Rev, 41, 6405-6447, Doi 10.1039/C2cs35181a, 2012.

Brown, S. S., Dube, W. P., Tham, Y. J., Zha, Q. Z., Xue, L. K., Poon, S., Wang, Z., Blake, D. R., Tsui, W., Parrish, D. D., and Wang, T.: Nighttime chemistry at a high altitude site above Hong Kong, Journal of Geophysical Research-Atmospheres, 121, 2457-2475, 10.1002/2015jd024566, 2016.

Chen, X., Wang, H., Lu, K., Li, C., Zhai, T., Tan, Z., Ma, X., Yang, X., Liu, Y., Chen, S., Dong, H., Li, X., Wu, Z., Hu, M., Zeng, L., and Zhang, Y.: Field Determination of Nitrate Formation Pathway in Winter Beijing, Environmental Science & Technology, 54, 9243-9253, 10.1021/acs.est.0c00972, 2020.

Chen, X., Wang, H., and Lu, K.: Interpretation of NO3–N2O5 observation via steady state in high-aerosol air mass: the impact of equilibrium coefficient in ambient conditions, Atmos. Chem. Phys., 22, 3525-3533, 10.5194/acp-22-3525-2022, 2022.

Clegg, S. L., Brimblecombe, P., and Wexler, A. S.: Thermodynamic model of the system H+-NH4+-SO42--NO3--H2O at tropospheric temperatures, J Phys Chem A, 102, 2137-2154, DOI 10.1021/jp973042r, 1998.

DeCarlo, P. F., Kimmel, J. R., Trimborn, A., Northway, M. J., Jayne, J. T., Aiken, A. C., Gonin, M.,

Fuhrer, K., Horvath, T., Docherty, K. S., Worsnop, D. R., and Jimenez, J. L.: Field-deployable, high-resolution, time-of-flight aerosol mass spectrometer, Analytical Chemistry, 78, 8281-8289, 10.1021/ac061249n, 2006.

Dong, H. B., Zeng, L. M., Hu, M., Wu, Y. S., Zhang, Y. H., Slanina, J., Zheng, M., Wang, Z. F., and Jansen, R.: Technical Note: The application of an improved gas and aerosol collector for ambient air pollutants in China, Atmospheric Chemistry and Physics, 12, 10519-10533, 10.5194/acp-12-10519-2012, 2012.

Eger, P. G., Friedrich, N., Schuladen, J., Shenolikar, J., Fischer, H., Tadic, I., Harder, H., Martinez, M., Rohloff, R., Tauer, S., Drewnick, F., Fachinger, F., Brooks, J., Darbyshire, E., Sciare, J., Pikridas, M., Lelieveld, J., and Crowley, J. N.: Shipborne measurements of ClNO2 in the Mediterranean Sea and around the Arabian Peninsula during summer, Atmospheric Chemistry and Physics, 19, 12121-12140, 10.5194/acp-19-12121-2019, 2019.

Evans, M. J., and Jacob, D. J.: Impact of new laboratory studies of N2O5 hydrolysis on global model budgets of tropospheric nitrogen oxides, ozone, and OH, Geophysical Research Letters, 32, Artn L09813

Doi 10.1029/2005gl022469, 2005.

Faxon, C. B., Bean, J. K., and Hildebrandt Ruiz, L.: Inland Concentrations of Cl-2 and ClNO2 in Southeast Texas Suggest Chlorine Chemistry Significantly Contributes to Atmospheric Reactivity, Atmosphere, 6, 1487-1506, 10.3390/atmos6101487, 2015.

Finlaysonpitts, B. J., Ezell, M. J., and Pitts, J. N.: Formation of Chemically Active Chlorine Compounds by Reactions of Atmospheric Nacl Particles with Gaseous N2o5 and Clono2, Nature, 337, 241-244, Doi 10.1038/337241a0, 1989.

Gaston, C. J., Thornton, J. A., and Ng, N. L.: Reactive uptake of N2O5 to internally mixed inorganic and organic particles: the role of organic carbon oxidation state and inferred organic phase separations, Atmospheric Chemistry and Physics, 14, 5693-5707, 10.5194/acp-14-5693-2014, 2014.

Ghosh, B., Papanastasiou, D. K., Talukdar, R. K., Roberts, J. M., and Burkholder, J. B.: Nitryl Chloride (ClNO2): UV/Vis Absorption Spectrum between 210 and 296 K and O(P-3) Quantum Yield at 193 and 248 nm, J Phys Chem A, 116, 5796-5805, 10.1021/jp207389y, 2012.

Hallquist, M., Stewart, D. J., Stephenson, S. K., and Cox, R. A.: Hydrolysis of N2O5 on sub-micron sulfate aerosols, Phys Chem Chem Phys, 5, 3453-3463, Doi 10.1039/B301827j, 2003.

Haskins, J. D., Lee, B. H., Lopez-Hilifiker, F. D., Peng, Q. Y., Jaegle, L., Reeves, J. M., Schroder, J. C., Campuzano-Jost, P., Fibiger, D., McDuffie, E. E., Jimenez, J. L., Brown, S. S., and Thornton, J. A.: Observational Constraints on the Formation of Cl-2 From the Reactive Uptake of ClNO2 on Aerosols in the Polluted Marine Boundary Layer, Journal of Geophysical Research-Atmospheres, 124, 8851-8869, 10.1029/2019jd030627, 2019.

He, X., Yuan, B., Wu, C., Wang, S., Wang, C., Huangfu, Y., Qi, J., Ma, N., Xu, W., Wang, M., Chen, W., Su, H., Cheng, Y., and Shao, M.: Volatile organic compounds in wintertime North China Plain: Insights from measurements of proton transfer reaction time-of-flight mass spectrometer (PTR-ToF-MS), Journal of Environmental Sciences, 114, 98-114, https://doi.org/10.1016/j.jes.2021.08.010, 2022.

Jeong, D., Seco, R., Gu, D., Lee, Y., Nault, B. A., Knote, C. J., McGee, T., Sullivan, J. T., Jimenez, J. L., Campuzano-Jost, P., Blake, D. R., Sanchez, D., Guenther, A. B., Tanner, D., Huey, L. G., Long,

766 R., Anderson, B. E., Hall, S. R., Ullmann, K., Shin, H., Herndon, S. C., Lee, Y., Kim, D., Ahn, J., and
767 Kim, S.: Integration of airborne and ground observations of nitryl chloride in the Seoul metropolitan
768 area and the implications on regional oxidation capacity during KORUS-AQ 2016, Atmos. Chem.
769 Phys., 19, 12779-12795, 10.5194/acp-19-12779-2019, 2019.
770 Le Breton, M., Hallquist, A. M., Pathak, R. K., Simpson, D., Wang, Y. J., Johansson, J., Zheng, J.,
771 Yang, Y. D., Shang, D. J., Wang, H. C., Liu, Q. Y., Chan, C., Wang, T., Bannan, T. J., Priestley, M.,
772 Percival, C. J., Shallcross, D. E., Lu, K. D., Guo, S., Hu, M., and Hallquist, M.: Chlorine oxidation
773 of VOCs at a semi-rural site in Beijing: significant chlorine liberation from ClNO2 and subsequent
774 gas- and particle-phase Cl-VOC production, Atmospheric Chemistry and Physics, 18, 13013-13030,
775 10.5194/acp-18-13013-2018, 2018.
776 Li, Q., Fu, X., Peng, X., Wang, W., Badia, A., Fernandez, R. P., Cuevas, C. A., Mu, Y., Chen, J.,
777 Jimenez, J. L., Wang, T., and Saiz-Lopez, A.: Halogens Enhance Haze Pollution in China,
778 Environmental Science & Technology, 55, 13625-13637, 10.1021/acs.est.1c01949, 2021.
779 Li, Q. Y., Zhang, L., Wang, T., Tham, Y. J., Ahmadov, R., Xue, L. K., Zhang, Q., and Zheng, J. Y.:
780 Impacts of heterogeneous uptake of dinitrogen pentoxide and chlorine activation on ozone and
781 reactive nitrogen partitioning: improvement and application of the WRF-Chem model in southern
782 China, Atmospheric Chemistry and Physics, 16, 14875-14890, 10.5194/acp-16-14875-2016, 2016.
783 Li, Q. Y., Borge, R., Sarwar, G., de la Paz, D., Gantt, B., Domingo, J., Cuevas, C. A., and Saiz-Lopez,
784 A.: Impact of halogen chemistry on summertime air quality in coastal and continental Europe:
785 application of the CMAQ model and implications for regulation, Atmospheric Chemistry and
786 Physics, 19, 15321-15337, 10.5194/acp-19-15321-2019, 2019.
787 Liu, X. G., Gu, J. W., Li, Y. P., Cheng, Y. F., Qu, Y., Han, T. T., Wang, J. L., Tian, H. Z., Chen, J., and
788 Zhang, Y. H.: Increase of aerosol scattering by hygroscopic growth: Observation, modeling, and
789 implications on visibility, Atmospheric Research, 132, 91-101, 10.1016/j.atmosres.2013.04.007,
790 2013.
791 Liu, X. X., Qu, H., Huey, L. G., Wang, Y. H., Sjostedt, S., Zeng, L. M., Lu, K. D., Wu, Y. S., Ho, M.,
792 Shao, M., Zhu, T., and Zhang, Y. H.: High Levels of Daytime Molecular Chlorine and Nitryl
793 Chloride at a Rural Site on the North China Plain, Environmental Science & Technology, 51, 9588-
794 9595, 10.1021/acs.est.7b03039, 2017.
795 Lou, S., Tan, Z., Gan, G., Chen, J., Wang, H., Gao, Y., Huang, D., Huang, C., Li, X., Song, R., Wang,
796 H., Wang, M., Wang, Q., Wu, Y., and Huang, C.: Observation based study on atmospheric oxidation
797 capacity in Shanghai during late-autumn: Contribution from nitryl chloride, Atmospheric
798 Environment, 271, 10.1016/j.atmosenv.2021.118902, 2022.
799 Lu, K. D., Rohrer, F., Holland, F., Fuchs, H., Bohn, B., Brauers, T., Chang, C. C., Haseler, R., Hu, M.,
800 Kita, K., Kondo, Y., Li, X., Lou, S. R., Nehr, S., Shao, M., Zeng, L. M., Wahner, A., Zhang, Y. H.,
801 and Hofzumahaus, A.: Observation and modelling of OH and HO2 concentrations in the Pearl River
802 Delta 2006: a missing OH source in a VOC rich atmosphere, Atmospheric Chemistry and Physics, 12,
803 1541-1569, 10.5194/acp-12-1541-2012, 2012.
804 McDuffie, E. E., Fibiger, D. L., Dube, W. P., Hilfiker, F. L., Lee, B. H., Jaegle, L., Guo, H. Y., Weber,
805 R. J., Reeves, J. M., Weinheimer, A. J., Schroder, J. C., Campuzano-Jost, P., Jimenez, J. L., Dibb, J.
806 E., Veres, P., Ebben, C., Sparks, T. L., Wooldridge, P. J., Cohen, R. C., Campos, T., Hall, S. R.,
807 Ullmann, K., Roberts, J. M., Thornton, J. A., and Brown, S. S.: ClNO2 Yields From Aircraft

Measurements During the 2015 WINTER Campaign and Critical Evaluation of the Current Parameterization, Journal of Geophysical Research-Atmospheres, 123, 12994-13015, 10.1029/2018JD029358, 2018a.

McDuffie, E. E., Fibiger, D. L., Dube, W. P., Lopez-Hilfiker, F., Lee, B. H., Thornton, J. A., Shah, V., Jaegle, L., Guo, H. Y., Weber, R. J., Reeves, J. M., Weinheimer, A. J., Schroder, J. C., Campuzano-Jost, P., Jimenez, J. L., Dibb, J. E., Veres, P., Ebben, C., Sparks, T. L., Wooldridge, P. J., Cohen, R. C., Hornbrook, R. S., Apel, E. C., Campos, T., Hall, S. R., Ullmann, K., and Brown, S. S.: Heterogeneous N2O5 Uptake During Winter: Aircraft Measurements During the 2015 WINTER Campaign and Critical Evaluation of Current Parameterizations, Journal of Geophysical Research-Atmospheres, 123, 4345-4372, 10.1002/2018jd028336, 2018b.

Mentel, T. F., Sohn, M., and Wahner, A.: Nitrate effect in the heterogeneous hydrolysis of dinitrogen pentoxide on aqueous aerosols, Phys Chem Chem Phys, 1, 5451-5457, Doi 10.1039/A905338g, 1999.

Mielke, L. H., Stutz, J., Tsai, C., Hurlock, S. C., Roberts, J. M., Veres, P. R., Froyd, K. D., Hayes, P. L., Cubison, M. J., Jimenez, J. L., Washenfelder, R. A., Young, C. J., Gilman, J. B., de Gouw, J. A., Flynn, J. H., Grossberg, N., Lefer, B. L., Liu, J., Weber, R. J., and Osthoff, H. D.: Heterogeneous formation of nitryl chloride and its role as a nocturnal NOx reservoir species during CalNex-LA 2010, Journal of Geophysical Research-Atmospheres, 118, 10638-10652, Doi 10.1002/Jgrd.50783, 2013.

Mielke, L. H., Furgeson, A., Odame-Ankrah, C. A., and Osthoff, H. D.: Ubiquity of ClNO2 in the urban boundary layer of Calgary, Alberta, Canada, Canadian Journal of Chemistry, 94, 414-423, 10.1139/cjc-2015-0426, 2015.

Mozurkewich, M., and Calvert, J. G.: Reaction Probability of N2o5 on Aqueous Aerosols, Journal of Geophysical Research-Atmospheres, 93, 15889-15896, DOI 10.1029/JD093iD12p15889, 1988.

Osthoff, H. D., Roberts, J. M., Ravishankara, A. R., Williams, E. J., Lerner, B. M., Sommariva, R., Bates, T. S., Coffman, D., Quinn, P. K., Dibb, J. E., Stark, H., Burkholder, J. B., Talukdar, R. K., Meagher, J., Fehsenfeld, F. C., and Brown, S. S.: High levels of nitryl chloride in the polluted subtropical marine boundary layer, Nat Geosci, 1, 324-328, Doi 10.1038/Ngeo177, 2008.

Peng, X., Wang, W., Xia, M., Chen, H., Ravishankara, A. R., Li, Q., Saiz-Lopez, A., Liu, P., Zhang, F., Zhang, C., Xue, L., Wang, X., George, C., Wang, J., Mu, Y., Chen, J., and Wang, T.: An unexpected large continental source of reactive bromine and chlorine with significant impact on wintertime air quality, Natl Sci Rev, 8, 10.1093/nsr/nwaa304, 2021.

Phillips, G. J., Tang, M. J., Thieser, J., Brickwedde, B., Schuster, G., Bohn, B., Lelieveld, J., and Crowley, J. N.: Significant concentrations of nitryl chloride observed in rural continental Europe associated with the influence of sea salt chloride and anthropogenic emissions, Geophysical Research Letters, 39, Artn L10811
10.1029/2012gl051912, 2012.

Phillips, G. J., Thieser, J., Tang, M. J., Sobanski, N., Schuster, G., Fachinger, J., Drewnick, F., Borrmann, S., Bingemer, H., Lelieveld, J., and Crowley, J. N.: Estimating N2O5 uptake coefficients using ambient measurements of NO3, N2O5, ClNO2 and particle-phase nitrate, Atmospheric Chemistry and Physics, 16, 13231-13249, 10.5194/acp-16-13231-2016, 2016.

Riedel, T. P., Bertram, T. H., Crisp, T. A., Williams, E. J., Lerner, B. M., Vlasenko, A., Li, S. M., Gilman, J., de Gouw, J., Bon, D. M., Wagner, N. L., Brown, S. S., and Thornton, J. A.: Nitryl

Chloride and Molecular Chlorine in the Coastal Marine Boundary Layer, Environmental Science & Technology, 46, 10463-10470, 10.1021/es204632r, 2012.

Riedel, T. P., Wagner, N. L., Dube, W. P., Middlebrook, A. M., Young, C. J., Ozturk, F., Bahreini, R., VandenBoer, T. C., Wolfe, D. E., Williams, E. J., Roberts, J. M., Brown, S. S., and Thornton, J. A.: Chlorine activation within urban or power plant plumes: Vertically resolved ClNO2 and Cl-2 measurements from a tall tower in a polluted continental setting, Journal of Geophysical Research-Atmospheres, 118, 8702-8715, 10.1002/jgrd.50637, 2013.

Riedel, T. P., Wolfe, G. M., Danas, K. T., Gilman, J. B., Kuster, W. C., Bon, D. M., Vlasenko, A., Li, S. M., Williams, E. J., Lerner, B. M., Veres, P. R., Roberts, J. M., Holloway, J. S., Lefer, B., Brown, S. S., and Thornton, J. A.: An MCM modeling study of nitryl chloride (ClNO2) impacts on oxidation, ozone production and nitrogen oxide partitioning in polluted continental outflow, Atmospheric Chemistry and Physics, 14, 3789-3800, 10.5194/acp-14-3789-2014, 2014.

Roberts, J. M., Osthoff, H. D., Brown, S. S., Ravishankara, A. R., Coffman, D., Quinn, P., and Bates, T.: Laboratory studies of products of N2O5 uptake on Cl- containing substrates, Geophysical Research Letters, 36, Artn L20808
10.1029/2009gl040448, 2009.

Ryder, O. S., Campbell, N. R., Shaloski, M., Al-Mashat, H., Nathanson, G. M., and Bertram, T. H.: Role of Organics in Regulating ClNO2 Production at the Air-Sea Interface, J Phys Chem A, 119, 8519-8526, 10.1021/jp5129673, 2015.

Saiz-Lopez, A., and von Glasow, R.: Reactive halogen chemistry in the troposphere, Chem Soc Rev, 41, 6448-6472, 2012.

Sarwar, G., Simon, H., Xing, J., and Mathur, R.: Importance of tropospheric ClNO2 chemistry across the Northern Hemisphere, Geophysical Research Letters, 41, 4050-4058, 10.1002/2014gl059962, 2014.

Shi, B., Wang, W., Zhou, L., Sun, Z., Fan, C., Chen, Y., Zhang, W., Qiao, Y., Qiao, Y., and Ge, M.: Atmospheric oxidation of C10~14 n-alkanes initiated by Cl atoms: Kinetics and mechanism, Atmospheric Environment, 222, 10.1016/j.atmosenv.2019.117166, 2020.

Simpson, W. R., Brown, S. S., Saiz-Lopez, A., Thornton, J. A., and von Glasow, R.: Tropospheric Halogen Chemistry: Sources, Cycling, and Impacts, Chemical Reviews, 115, 4035-4062, 10.1021/cr5006638, 2015.

Sommariva, R., Hollis, L. D. J., Sherwen, T., Baker, A. R., Ball, S. M., Bandy, B. J., Bell, T. G., Chowdhury, M. N., Cordell, R. L., Evans, M. J., Lee, J. D., Reed, C., Reeves, C. E., Roberts, J. M., Yang, M. X., and Monks, P. S.: Seasonal and geographical variability of nitryl chloride and its precursors in Northern Europe, Atmos Sci Lett, 19, UNSP e844
10.1002/asl.844, 2018.

Staudt, S., Gord, J. R., Karimova, N. V., McDuffie, E. E., Brown, S. S., Gerber, R. B., Nathanson, G. M., and Bertram, T. H.: Sulfate and Carboxylate Suppress the Formation of ClNO2 at Atmospheric Interfaces, Acs Earth Space Chem, 3, 1987-1997, 10.1021/acsearthspacechem.9b00177, 2019.

Tan, Z., Fuchs, H., Lu, K., Hofzumahaus, A., Bohn, B., Broch, S., Dong, H., Gomm, S., Haeseler, R., He, L., Holland, F., Li, X., Liu, Y., Lu, S., Rohrer, F., Shao, M., Wang, B., Wang, M., Wu, Y., Zeng, L., Zhang, Y., Wahner, A., and Zhang, Y.: Radical chemistry at a rural site (Wangdu) in the North China Plain: observation and model calculations of OH, HO2 and RO2 radicals, Atmospheric

Chemistry and Physics, 17, 663-690, 10.5194/acp-17-663-2017, 2017.

Tan, Z. F., Lu, K. D., Hofzumahaus, A., Fuchs, H., Bohn, B., Holland, F., Liu, Y. H., Rohrer, F., Shao, M., Sun, K., Wu, Y. S., Zeng, L. M., Zhang, Y. S., Zou, Q., Kiendler-Scharr, A., Wahner, A., and Zhang, Y. H.: Experimental budgets of OH, HO2, and RO2 radicals and implications for ozone formation in the Pearl River Delta in China 2014, Atmospheric Chemistry and Physics, 19, 7129-7150, 10.5194/acp-19-7129-2019, 2019.

Tang, M. J., Telford, P. J., Pope, F. D., Rkiouak, L., Abraham, N. L., Archibald, A. T., Braesicke, P., Pyle, J. A., McGregor, J., Watson, I. M., Cox, R. A., and Kalberer, M.: Heterogeneous reaction of N2O5 with airborne TiO2 particles and its implication for stratospheric particle injection, Atmospheric Chemistry and Physics, 14, 6035-6048, DOI 10.5194/acp-14-6035-2014, 2014.

Thaler, R. D., Mielke, L. H., and Osthoff, H. D.: Quantification of Nitryl Chloride at Part Per Trillion Mixing Ratios by Thermal Dissociation Cavity Ring-Down Spectroscopy, Analytical Chemistry, 83, 2761-2766, 10.1021/ac200055z, 2011.

Tham, Y. J., Yan, C., Xue, L. K., Zha, Q. Z., Wang, X. F., and Wang, T.: Presence of high nitryl chloride in Asian coastal environment and its impact on atmospheric photochemistry, Chinese Science Bulletin, 59, 356-359, 10.1007/s11434-013-0063-y, 2014.

Tham, Y. J., Wang, Z., Li, Q. Y., Yun, H., Wang, W. H., Wang, X. F., Xue, L. K., Lu, K. D., Ma, N., Bohn, B., Li, X., Kecorius, S., Gross, J., Shao, M., Wiedensohler, A., Zhang, Y. H., and Wang, T.: Significant concentrations of nitryl chloride sustained in the morning: investigations of the causes and impacts on ozone production in a polluted region of northern China, Atmospheric Chemistry and Physics, 16, 14959-14977, 10.5194/acp-16-14959-2016, 2016.

Tham, Y. J., Wang, Z., Li, Q. Y., Wang, W. H., Wang, X. F., Lu, K. D., Ma, N., Yan, C., Kecorius, S., Wiedensohler, A., Zhang, Y. H., and Wang, T.: Heterogeneous N2O5 uptake coefficient and production yield of ClNO2 in polluted northern China: roles of aerosol water content and chemical composition, Atmospheric Chemistry and Physics, 18, 13155-13171, 10.5194/acp-18-13155-2018, 2018.

Thornton, J. A., Kercher, J. P., Riedel, T. P., Wagner, N. L., Cozic, J., Holloway, J. S., Dube, W. P., Wolfe, G. M., Quinn, P. K., Middlebrook, A. M., Alexander, B., and Brown, S. S.: A large atomic chlorine source inferred from mid-continental reactive nitrogen chemistry, Nature, 464, 271-274, 10.1038/nature08905, 2010a.

Thornton, J. A., Kercher, J. P., Riedel, T. P., Wagner, N. L., Cozic, J., Holloway, J. S., Dube, W. P., Wolfe, G. M., Quinn, P. K., Middlebrook, A. M., Alexander, B., and Brown, S. S.: A large atomic chlorine source inferred from mid-continental reactive nitrogen chemistry, Nature, 464, 271-274, 10.1038/nature08905, 2010b.

Veres, P. R., Neuman, J. A., Bertram, T. H., Assaf, E., Wolfe, G. M., Williamson, C. J., Weinzierl, B., Tilmes, S., Thompson, C. R., Thames, A. B., Schroder, J. C., Saiz-Lopez, A., Rollins, A. W., Roberts, J. M., Price, D., Peischl, J., Nault, B. A., Moller, K. H., Miller, D. O., Meinardi, S., Li, Q., Lamarque, J. F., Kupc, A., Kjaergaard, H. G., Kinnison, D., Jimenez, J. L., Jernigan, C. M., Hornbrook, R. S., Hills, A., Dollner, M., Day, D. A., Cuevas, C. A., Campuzano-Jost, P., Burkholder, J., Bui, T. P., Brune, W. H., Brown, S. S., Brock, C. A., Bourgeois, I., Blake, D. R., Apel, E. C., and Ryerson, T. B.: Global airborne sampling reveals a previously unobserved dimethyl sulfide oxidation mechanism in the marine atmosphere, Proc Natl Acad Sci U S A, 117, 4505-4510, 10.1073/pnas.1919344117, 2020.

934 Wagner, N. L., Riedel, T. P., Roberts, J. M., Thornton, J. A., Angevine, W. M., Williams, E. J., Lerner,
935 B. M., Vlasenko, A., Li, S. M., Dube, W. P., Coffman, D. J., Bon, D. M., de Gouw, J. A., Kuster, W.
936 C., Gilman, J. B., and Brown, S. S.: The sea breeze/land breeze circulation in Los Angeles and its
937 influence on nitryl chloride production in this region, Journal of Geophysical Research-Atmospheres,
938 117, Artn D00v24
939 10.1029/2012jd017810, 2012.
940 Wahner, A., Mentel, T. F., Sohn, M., and Stier, J.: Heterogeneous reaction of N2O5 on sodium nitrate
941 aerosol, Journal of Geophysical Research-Atmospheres, 103, 31103-31112, Doi
942 10.1029/1998jd100022, 1998.
943 Wang, H., Lu, K., Chen, X., Zhu, Q., Chen, Q., Guo, S., Jiang, M., Li, X., Shang, D., Tan, Z., Wu, Y.,
944 Wu, Z., Zou, Q., Zheng, Y., Zeng, L., Zhu, T., Hu, M., and Zhang, Y.: High N2O5 Concentrations
945 Observed in Urban Beijing: Implications of a Large Nitrate Formation Pathway, Environmental
946 Science & Technology Letters, 4, 416-420, 10.1021/acs.estlett.7b00341, 2017a.
947 Wang, H., Lu, K., Tan, Z., Sun, K., Li, X., Hu, M., Shao, M., Zeng, L., Zhu, T., and Zhang, Y.: Model
948 simulation of NO3, N2O5 and ClNO2 at a rural site in Beijing during CAREBeijing-2006,
949 Atmospheric Research, 196, 97-107, 10.1016/j.atmosres.2017.06.013, 2017b.
950 Wang, H., Lu, K., Guo, S., Wu, Z., Shang, D., Tan, Z., Wang, Y., Le Breton, M., Lou, S., Tang, M.,
951 Wu, Y., Zhu, W., Zheng, J., Zeng, L., Hallquist, M., Hu, M., and Zhang, Y.: Efficient N2O5 uptake
952 and NO3 oxidation in the outflow of urban Beijing, Atmospheric Chemistry and Physics, 18, 9705-
953 9721, 10.5194/acp-18-9705-2018, 2018.
954 Wang, H., and Lu, K.: Monitoring Ambient Nitrate Radical by Open-Path Cavity-Enhanced
955 Absorption Spectroscopy, Analytical Chemistry, 91, 10687-10693, 10.1021/acs.analchem.9b01971,
956 2019.
957 Wang, H., Chen, X., Lu, K., Tan, Z., Ma, X., Wu, Z., Li, X., Liu, Y., Shang, D., Wu, Y., Zeng, L., Hu,
958 M., Schmitt, S., Kiendler-Scharr, A., Wahner, A., and Zhang, Y.: Wintertime N2O5 uptake
959 coefficients over the North China Plain, Science Bulletin, 65, 765-774, 10.1016/j.scib.2020.02.006,
960 2020a.
961 Wang, H., Peng, C., Wang, X., Lou, S., Lu, K., Gan, G., Jia, X., Chen, X., Chen, J., Wang, H., Fan, S.,
962 Wang, X., and Tang, M.: N$_2$O$_5$ uptake onto saline mineral dust: a
963 potential missing source of tropospheric ClNO$_2$ in inland China, Atmospheric
964 Chemistry and Physics, 22, 1845-1859, 10.5194/acp-22-1845-2022, 2022a.
965 Wang, K., Wang, W., Fan, C., Li, J., Lei, T., Zhang, W., Shi, B., Chen, Y., Liu, M., Lian, C., Wang, Z.,
966 and Ge, M.: Reactions of C12–C14 n-Alkylcyclohexanes with Cl Atoms: Kinetics and Secondary
967 Organic Aerosol Formation, Environmental Science & Technology, 56, 4859-4870,
968 10.1021/acs.est.1c08958, 2022b.
969 Wang, T., Tham, Y. J., Xue, L. K., Li, Q. Y., Zha, Q. Z., Wang, Z., Poon, S. C. N., Dube, W. P., Blake,
970 D. R., Louie, P. K. K., Luk, C. W. Y., Tsui, W., and Brown, S. S.: Observations of nitryl chloride and
971 modeling its source and effect on ozone in the planetary boundary layer of southern China, Journal
972 of Geophysical Research-Atmospheres, 121, 2476-2489, 10.1002/2015jd024556, 2016.
973 Wang, T., Dai, J. N., Lam, K. S., Poon, C. N., and Brasseur, G. P.: Twenty-Five Years of Lower
974 Tropospheric Ozone Observations in Tropical East Asia: The Influence of Emissions and Weather
975 Patterns, Geophysical Research Letters, 46, 11463-11470, 10.1029/2019gl084459, 2019a.

Wang, W., Yuan, B., Peng, Y., Su, H., Cheng, Y., Yang, S., Wu, C., Qi, J., Bao, F., Huangfu, Y., Wang, C., Ye, C., Wang, Z., Wang, B., Wang, X., Song, W., Hu, W., Cheng, P., Zhu, M., Zheng, J., and Shao, M.: Direct observations indicate photodegradable oxygenated volatile organic compounds (OVOCs) as larger contributors to radicals and ozone production in the atmosphere, Atmospheric Chemistry and Physics, 22, 4117-4128, 10.5194/acp-22-4117-2022, 2022c.

Wang, X., Jacob, D. J., Eastham, S. D., Sulprizio, M. P., Zhu, L., Chen, Q., Alexander, B., Sherwen, T., Evans, M. J., Lee, B. H., Haskins, J. D., Lopez-Hilfiker, F. D., Thornton, J. A., Huey, G. L., and Liao, H.: The role of chlorine in global tropospheric chemistry, Atmospheric Chemistry and Physics, 19, 3981-4003, 10.5194/acp-19-3981-2019, 2019b.

Wang, X., Jacob, D. J., Eastham, S. D., Sulprizio, M. P., Zhu, L., Chen, Q. J., Alexander, B., Sherwen, T., Evans, M. J., Lee, B. H., Haskins, J. D., Lopez-Hilfiker, F. D., Thornton, J. A., Huey, G. L., and Liao, H.: The role of chlorine in global tropospheric chemistry, Atmospheric Chemistry and Physics, 19, 3981-4003, 10.5194/acp-19-3981-2019, 2019c.

Wang, X. F., Wang, H., Xue, L. K., Wang, T., Wang, L. W., Gu, R. R., Wang, W. H., Tham, Y. J., Wang, Z., Yang, L. X., Chen, J. M., and Wang, W. X.: Observations of N2O5 and ClNO2 at a polluted urban surface site in North China: High N2O5 uptake coefficients and low ClNO2 product yields, Atmospheric Environment, 156, 125-134, 10.1016/j.atmosenv.2017.02.035, 2017c.

Wang, Z., Wang, W. H., Tham, Y. J., Li, Q. Y., Wang, H., Wen, L., Wang, X. F., and Wang, T.: Fast heterogeneous N2O5 uptake and ClNO2 production in power plant and industrial plumes observed in the nocturnal residual layer over the North China Plain, Atmospheric Chemistry and Physics, 17, 12361-12378, 10.5194/acp-17-12361-2017, 2017d.

Wang, Z., Yuan, B., Ye, C., Roberts, J., Wisthaler, A., Lin, Y., Li, T., Wu, C., Peng, Y., Wang, C., Wang, S., Yang, S., Wang, B., Qi, J., Wang, C., Song, W., Hu, W., Wang, X., Xu, W., Ma, N., Kuang, Y., Tao, J., Zhang, Z., Su, H., Cheng, Y., Wang, X., and Shao, M.: High Concentrations of Atmospheric Isocyanic Acid (HNCO) Produced from Secondary Sources in China, Environmental Science & Technology, 54, 11818-11826, 10.1021/acs.est.0c02843, 2020b.

Wu, C., Wang, C., Wang, S., Wang, W., Yuan, B., Qi, J., Wang, B., Wang, H., Wang, C., Song, W., Wang, X., Hu, W., Lou, S., Ye, C., Peng, Y., Wang, Z., Huangfu, Y., Xie, Y., Zhu, M., Zheng, J., Wang, X., Jiang, B., Zhang, Z., and Shao, M.: Measurement report: Important contributions of oxygenated compounds to emissions and chemistry of volatile organic compounds in urban air, Atmos. Chem. Phys., 20, 14769-14785, 10.5194/acp-20-14769-2020, 2020.

Xia, M., Peng, X., Wang, W., Yu, C., Sun, P., Li, Y., Liu, Y., Xu, Z., Wang, Z., Xu, Z., Nie, W., Ding, A., and Wang, T.: Significant production of ClNO$_2$ and possible source of Cl$_2$ from N$_2$O$_5$ uptake at a suburban site in eastern China, Atmospheric Chemistry and Physics, 20, 6147-6158, 10.5194/acp-20-6147-2020, 2020.

Xia, M., Peng, X., Wang, W. H., Yu, C. A., Wang, Z., Tham, Y. J., Chen, J. M., Chen, H., Mu, Y. J., Zhang, C. L., Liu, P. F., Xue, L. K., Wang, X. F., Gao, J., Li, H., and Wang, T.: Winter ClNO2 formation in the region of fresh anthropogenic emissions: seasonal variability and insights into daytime peaks in northern China, Atmospheric Chemistry and Physics, 21, 15985-16000, 10.5194/acp-21-15985-2021, 2021.

Xue, L. K., Saunders, S. M., Wang, T., Gao, R., Wang, X. F., Zhang, Q. Z., and Wang, W. X.:

Development of a chlorine chemistry module for the Master Chemical Mechanism, Geoscientific Model Development, 8, 3151-3162, 10.5194/gmd-8-3151-2015, 2015.

Yang, S., Yuan, B., Peng, Y., Huang, S., Chen, W., Hu, W., Pei, C., Zhou, J., Parrish, D. D., Wang, W., He, X., Cheng, C., Li, X.-B., Yang, X., Song, Y., Wang, H., Qi, J., Wang, B., Wang, C., Wang, C., Wang, Z., Li, T., Zheng, E., Wang, S., Wu, C., Cai, M., Ye, C., Song, W., Cheng, P., Chen, D., Wang, X., Zhang, Z., Wang, X., Zheng, J., and Shao, M.: The formation and mitigation of nitrate pollution: comparison between urban and suburban environments, Atmospheric Chemistry and Physics, 22, 4539-4556, 10.5194/acp-22-4539-2022, 2022a.

Yang, X., Wang, T., Xia, M., Gao, X. M., Li, Q. Y., Zhang, N. W., Gao, Y., Lee, S. C., Wang, X. F., Xue, L. K., Yang, L. X., and Wang, W. X.: Abundance and origin of fine particulate chloride in continental China, Science of the Total Environment, 624, 1041-1051, 10.1016/j.scitotenv.2017.12.205, 2018.

Yang, X., Wang, Q., Ma, N., Hu, W., Gao, Y., Huang, Z., Zheng, J., Yuan, B., Yang, N., Tao, J., Hong, J., Cheng, Y., and Su, H.: The impact of chlorine chemistry combined with heterogeneous N_2O_5 reactions on air quality in China, Atmospheric Chemistry and Physics, 22, 3743-3762, 10.5194/acp-22-3743-2022, 2022b.

Ye, C., Yuan, B., Lin, Y., Wang, Z., Hu, W., Li, T., Chen, W., Wu, C., Wang, C., Huang, S., Qi, J., Wang, B., Wang, C., Song, W., Wang, X., Zheng, E., Krechmer, J. E., Ye, P., Zhang, Z., Wang, X., Worsnop, D. R., and Shao, M.: Chemical characterization of oxygenated organic compounds in the gas phase and particle phase using iodide CIMS with FIGAERO in urban air, Atmos. Chem. Phys., 21, 8455-8478, 10.5194/acp-21-8455-2021, 2021.

Young, C. J., Washenfelder, R. A., Roberts, J. M., Mielke, L. H., Osthoff, H. D., Tsai, C., Pikelnaya, O., Stutz, J., Veres, P. R., Cochran, A. K., VandenBoer, T. C., Flynn, J., Grossberg, N., Haman, C. L., Lefer, B., Stark, H., Graus, M., de Gouw, J., Gilman, J. B., Kuster, W. C., and Brown, S. S.: Vertically Resolved Measurements of Nighttime Radical Reservoirs; in Los Angeles and Their Contribution to the Urban Radical Budget, Environmental Science & Technology, 46, 10965-10973, 10.1021/es302206a, 2012.

Yu, C., Wang, Z., Xia, M., Fu, X., Wang, W., Tham, Y. J., Chen, T., Zheng, P., Li, H., Shan, Y., Wang, X., Xue, L., Zhou, Y., Yue, D., Ou, Y., Gao, J., Lu, K., Brown, S. S., Zhang, Y., and Wang, T.: Heterogeneous N2O5 reactions on atmospheric aerosols at four Chinese sites: improving model representation of uptake parameters, Atmos. Chem. Phys., 20, 4367-4378, 10.5194/acp-20-4367-2020, 2020.

Yun, H., Wang, T., Wang, W. H., Tham, Y. J., Li, Q. Y., Wang, Z., and Poon, S. C. N.: Nighttime NOx loss and ClNO2 formation in the residual layer of a polluted region: Insights from field measurements and an iterative box model, Science of the Total Environment, 622, 727-734, 10.1016/j.scitotenv.2017.11.352, 2018a.

Yun, H., Wang, W. H., Wang, T., Xia, M., Yu, C., Wang, Z., Poon, S. C. N., Yue, D. L., and Zhou, Y.: Nitrate formation from heterogeneous uptake of dinitrogen pentoxide during a severe winter haze in southern China, Atmospheric Chemistry and Physics, 18, 17515-17527, 10.5194/acp-18-17515-2018, 2018b.

Zhou, W., Zhao, J., Ouyang, B., Mehra, A., Xu, W. Q., Wang, Y. Y., Bannan, T. J., Worrall, S. D., Priestley, M., Bacak, A., Chen, Q., Xie, C. H., Wang, Q. Q., Wang, J. F., Du, W., Zhang, Y. J., Ge, X.

L., Ye, P. L., Lee, J. D., Fu, P. Q., Wang, Z. F., Worsnop, D., Jones, R., Percival, C. J., Coe, H., and Sun, Y. L.: Production of N2O5 and ClNO2 in summer in urban Beijing, China, Atmospheric Chemistry and Physics, 18, 11581-11597, 10.5194/acp-18-11581-2018, 2018.

Zong, T., Wang, H., Wu, Z., Lu, K., Wang, Y., Zhu, Y., Shang, D., Fang, X., Huang, X., He, L., Ma, N., GroSs, J., Huang, S., Guo, S., Zeng, L., Herrmann, H., Wiedensohler, A., Zhang, Y., and Hu, M.: Particle hygroscopicity inhomogeneity and its impact on reactive uptake, The Science of the total environment, 151364-151364, 10.1016/j.scitotenv.2021.151364, 2021.